ERROR SIMULATION AND ADAPTIVE MODE TUNING OF MICROMACHINED GYROSCOPES

A DISSERTATION

Submitted in partial fulfillment of the requirements for the award of the degree

of

MASTER OF TECHNOLOGY

in

ELECTRONICS AND COMMUNICATION ENGINEERING

(With Specialization in Control and Guidance)

By

WING COMMANDER R MUKESH

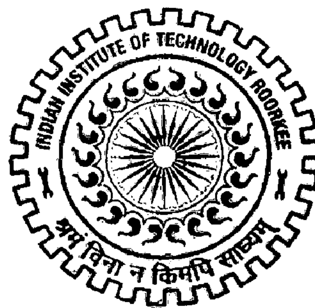

DEPARTMENT OF ELECTRONICS AND COMPUTER ENGINEERING
INDIAN INSTITUTE OF TECHNOLOGY ROORKEE
ROORKEE -247 667 (INDIA)

JUNE, 2009

CANDIDATE'S DECLARATION

I hereby declare that the work, which is presented in this dissertation report, titled "**Error simulation and adaptive mode tuning of Micromachined Gyroscopes**", being submitted in partial fulfillment of the requirements for the award of the degree of **Master of Technology** with specialization in **Control and Guidance**, in the Department of Electronics and Computer Engineering, Indian Institute of Technology, Roorkee is an authentic record of my own work carried out from July 2008 to June 2009, under guidance and supervision of **Dr. R. MITRA**, Professor, Department of Electronics and Computer Engineering, Indian Institute of Technology, Roorkee.

The results embodied in this dissertation have not submitted for the award of any other Degree or Diploma.

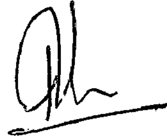

Date : 08 **Jun 09**

Place: Roorkee

R MUKESH

CERTIFICATE

This is to certify that the statement made by the candidate is correct to the best of my knowledge and belief.

(Dr. R. MITRA)

Professor, E&C Department,

Indian Institute of Technology, Roorkee

Roorkee 247667 (INDIA)

Date: 08 **Jun 09**

ACKNOWLEDGEMENTS

It is my privilege and pleasure to express my profound sense of respect, gratitude and indebtedness to my guide, Dr. R. MITRA, Professor, Department of Electronics and Computer Engineering , Indian Institute of Technology, Roorkee, for his inspiration, guidance, constructive criticisms and encouragement throughout this dissertation work.

Thanks are due to the Lab staff Control and Guidance Lab, Department of Electronics and Computer Engineering, IIT Roorkee for providing necessary facilities.

I gratefully acknowledge my sincere thanks to my family members for their inspirational words and moral support during course of this work.

I am greatly indebted to all my friends, who have graciously applied themselves to the task of helping me with ample morale support and valuable suggestions. Finally, I would like to extend my gratitude to all those persons who have directly or indirectly helped me in the process and contributed towards this work.

R MUKESH

ABSTRACT

Micromachined gyroscopes for measuring rate or angle of rotation have attracted a lot of attention during the past few years for several applications. Conventional rotating wheel as well as precision fiber optic and ring laser gyroscopes are all too expensive and too large for use in most emerging applications. Micromachined gyroscopes are mainly attractive because of their small size (~ 1 mm X 1 mm including sensing circuits) and low cost. Most microgyroscopes consist of a vibrating proof-mass which is driven into oscillation by electrostatic or other means. When placed in a rotational field, the vibrating proof-mass experiences an apparent force called the Coriolis force, which is proportional to the cross-product of the angular velocity of the rotational field and the translational velocity of the oscillating proof-mass.

Fabrication of micromachined gyroscopes involves multiple processing steps including deposition, etching and patterning of materials. Every fabrication step contribute to imperfections in the gyroscope. Imperfections are reflected in asymmetry and anisoelasticity of the structure. Asymmetries result in undesirable constantly acting perturbations in the form of mechanical and electrostatic forces. Simulation of non-idealities in micromachined gyroscopes is essential to understand its behaviour in the entire range of operation and formulate control strategies to counter the same.

In most MEMS gyroscopes, it is desirable to operate the drive axis vibration at the resonant frequency in order to obtain a large response and phase synchronization. Adaptive mode tuning as an alternate to phase locked loop so as to place the resonant frequency at a specified frequency is analysed and simulated to obtain better performance of gyroscope.

Contents

Candidate's Declaration And Certificate i
Acknowledgement ii
Abstract iii
List of Figures iv

1. INTRODUCTION

1.1 History 01
1.2 Motivation 06
1.3 Problem Statement 08
1.4 Outline of the dissertation 09

2. MICROMACHINING CONCEPTS

2.1 Introduction 10
2.2 Historical background 11
2.3 Mechanical properties of Silicon 13
2.4 Major branches of MEMS technology 14
2.5 Microelectronics Vs MEMS 15
2.6 Fabrication techniques 16
2.7 IC Fabrication 17
2.8 Bulk Micromachining and Wafer bonding 19
2.9 Surface Micromachining 20
2.10 LIGA process 22
2.11 Advantages of MEMS 24
2.12 Applications of MEMS 24
2.13 The Future of MEMS 24

3. MICROMACHINED GYROSCOPES

3.1 Operation principle 26
3.2 Classification of gyroscopes 27
3.3 Ideal dynamical system 29
3.4 Mode matching 32

4. SIMULATION OF ERRORS IN MM GYROSCOPES

4.1 Introduction 34
4.2 Modeling of imperfections 35
4.3 Off diagonal elements 37

4.4 Analysis of imperfections ____ 38
4.5 Motion decomposition ____ 39
4.6 Error classification ____ 41

5. CONTROL STRATEGIES

5.1 Introduction ____ 43
5.2 Quadrature Control ____ 44
5.3 Sliding mode controller ____ 48
5.4 Active Disturbance Rejection Controller ____ 50
5.5 Adaptive Mode Tuning for Vibrational Gyroscopes ____ 52
5.5.1 Gyroscope Drive Axis Model ____ 53
5.5.2 Resonant Gain ____ 54
5.5.3 Adaptive control for resonance ____ 55

6. SIMULATION RESULTS

6.1 Ideal gyroscope ____ 57
6.2 Non-idealities in gyroscope
6.2.1 Stiffness ____ 61
6.2.2 Damping ____ 64
6.3 Adaptive Mode Tuning
6.3.1 Adaptive tuning with linear phase detector ____ 67
6.3.2 Adaptive tuning with saturating phase detector ____ 68

7. CONCLUSION AND FUTURE SCOPE ____ 71

REFERENCES ____ 73

LIST OF FIGURES

Fig 2.10.1 Fabrication steps in the LIGA process ____________ 23
Fig 3.1 Operation principle of a gyroscope ____________ 27
Fig 3.2 Classification of vibratory gyroscope ____________ 27
Fig 3.3(a) Dynamic system for gyroscope ____________ 29
Fig 3.3(b) Trajectory of the vibrating mass in terms of the Orbital elements ____________ 29
Fig 3.4(a) Driving frequency versus Drive mode amplitude ____________ 33
Fig 3.4(b) Frequency versus Response amplitude ____________ 33
Fig 4.2.1 Ideal gyroscope ____________ 36
Fig 4.2.2 Anisoelasticity in gyroscope ____________ 36
Fig 5.2.1(a) Anisoelasticities result in quadrature error which manifests as a developing elliptical pattern during precession of the straight line oscillation. ____________ 47
Fig 5.2.1(b) Use of feedback control to compensate anisoelasticity while preserving the angle of precession φ ____________ 47
Fig 5.2.2(a) Larger errors in anisoelasticity resulting in erratic oscillations 48
Fig 5.2.2(b) Effect of feedback control to compensate larger errors ____ 48
Fig 5.3.1 Force balancing controller ____________ 49
Fig 5.5.1 Feedback loop with adaptive control gain $\hat{K}$ ____________ 54
Fig 6.1.1 MATLAB Editor result for ideal gyroscope ____________ 58
Fig 6.1.2 Orbital elements of a vibrating member ____________ 59
Fig 6.1.3 Ellipse motion of the point (x,y) when (a) a=1 and b=0 (b) a=20 and b=0 ____________ 59
Fig 6.1.4(a) Ellipse when a=20, b=10 (b) Circle when a=b=20 ____________ 60
Fig 6.2.1(a) Precession of straight line due to non-zero off diagonal terms in stiffness matrix ____________ 61
Fig 6.2.1(b) With 1 per cent variation in the off-diagonal elements, the plot of (x,y) is a precessing ellipsoid instead of a straight line ____________ 62
Fig 6.2.1(c) Variation of 5% in the off-diagonal elements____________ 63
Fig 6.2.1(d) Effect of non-potential forces due to unequal off-diagonal elements in the stiffness matrix.____________ 64
Fig 6.2.2(a) Hyperbolic velocity dependent forces due to damping results in precession of the straight line oscillation and amplitude change 65
Fig 6.2.2(b) Effect of gyroscopic force in damping matrix ____________ 66
Figure 6.3.1 Adaptive tuning with linear phase detector and no low pass filter. Graph depicts $\hat{K}$ versus time ____________ 67
Fig 6.3.2 Adaptive tuning with linear phase detector and no low pass filter. Error i/p vs time (XY Graph1) & filtered o/p vs time (XYGraph) ____ 68
Figure 6.3.3 Adaptive tuning with saturation phase detector and a low pass filter. Graph depicts $\hat{K}$ versus time ____________ 69
Figure 6.3.4 Adaptive tuning with saturation phase detector and a low pass filter. Graph depicts error input vs time ____________ 69

Introduction

Automatic navigation [1] makes ocean going and flying safer and less expensive: Safer, because machines are tireless and always vigilant; inexpensive because it does not require human navigators who are, unavoidably, highly trained and thus expensive people. Unmanned deep space travel would be impossible without automatic navigation. Navigation can be automated with the radio systems Loran, Omega and the Global Positioning Systems (GPS) of earth satellites. In some circumstances, such as when a submarine is deeply submerged or in a war zone where radio signals may be jammed, these aids are not available. Then a self contained system is used, which is called inertial navigation.

Inertial navigation uses gyroscopes and accelerometers (inertial sensors) to measure the state of motion of the vehicle by noting changes in that state caused by accelerations. By knowing the vehicle's starting position and noting the changes in its direction and speed, one can keep track of the vehicle's current position. Mankind first used this technology in World War II, in strategic guided weapons where cost was unimportant; only after two to three decades later did it become cheap enough to be used commercially.

1.1 History

To study the earth's rotation, the French scientist Leon Foucault used a large pendulum (67m long), which he built in the Pantheon in Paris. Its iron bob weighed 28 kg, and it swung with a period of about 15 seconds. As the earth rotated under the swinging pendulum, the plane of the swing appeared to rotate clockwise (because he was in the northern hemisphere) at vertical earth's rate because the pendulum's momentum was fixed in inertial space.

The pendulum motion was perturbed by draughts, so it soon became inaccurate as an inertial reference. Foucault devised a more compact and accurate instrument in 1852, a gimbaled wheel that, because of its angular momentum, would stay fixed in space while his laboratory rotated around it. Foucault joined the Greek words that mean "to view" and "rotation", *gyros* and *skopein*, and coined the word gyroscope for his suspended wheel. In this dissertation, this word is used for any instrument that signals or measures rotation.

In an 1851 paper [2], Foucault described the experiment that ultimately led to his celebrated pendulum. He discovered that the plane of transverse oscillation of a thin, vibrating rod clamped in the chuck of a lathe tends to remain fixed in space independent of the rotation of the chuck. This momentum conservation principle has been used as the basis of a class of gyroscopes in which the conventional inertia wheel is replaced by a vibrating member. An instrument of this class comprises, in addition to the vibrating member, an enclosure in which the vibrating member is suspended and a sensor to measure the angular displacement of the plane of vibration relative to the enclosure. This angular displacement indicates the angular rotation of the body to which the enclosure is attached.

Over the past century, the "modern" gyroscope has undergone a series of evolutionary processes to the gyroscopes we know today. The use of gyroscopes in navigation dates back to the early 1900's when gyrocompasses invented by Elmer Sperry were used by mariners to navigate on the open seas. By the 1950's, gimbaled gyroscope and accelerometer systems were realized for motion sensing in aircraft systems. As these systems provided an attitude reference system, it was not necessary to have high accuracy. Because of the complexity and cost of making a gimbaled attitude reference system, the idea of strapdown systems became popular in the 1970's.

To achieve adequate performance, however, the strap down systems required high accuracy gyroscopes with a drift of less than 0.01 deg/hr. To answer this call for accuracy, optical gyroscopes based on lasers propagating in a ring and in fiber-optic cable were created with superior accuracy and reliability. However, these high accuracy gyroscopes are bulky and expensive, and thus are reserved for use in mainly aircraft, naval and space applications. Thus, there is a need for a new class of gyroscopes, preferably micromachined. The past 40 years has seen the advent of micromachined inertial sensors, which allows gyroscopes and accelerometers to be built smaller, cheaper and using less power.

The field of Microelectromechanical systems (MEMS) has emerged as a technology [5] that promises to have significant impact on everyday living in the near future. MEMS provide inexpensive means to sense, and, in a limited way, control physical, chemical and biological interactions with nature. They add a new dimension to the information revolution of the latter half of the twentieth century, by enabling access to sensor data previously limited to industrial, military and medical applications. MEMS seek to achieve this vision through a variety of manufacturing techniques common among which are surface micromachining, bulk micromachining and LIGA. These, integrated circuit like techniques, are capable of producing micrometer-scale features. However, they lack the precision of traditional mechanical fabrication practices. Being integrated circuit compatible, they derive their power by leveraging well understood and characterized signal processing capabilities of integrated circuits. As a result, a wide spectrum of applications have been made possible such as inertial sensors, pressure and acoustic transducers, high frequency radios, optical communications, lab-on-a-chip for chemical and biological analysis.

This dissertation is primarily relevant for micromachined gyroscopes, which is an important part of the inertial sensing family devices. Multi-axial accelerometers and gyroscopes can be combined to build an inertial measurement unit (IMU), also called an Inertial Navigation System (INS). High precision IMUs have been

an indispensable part of ships, aeroplanes, satellites and space shuttles and the like. The availability of low cost inertial sensors has opened up a wide range of new applications which do no require the high precision that IMUs demand. Air-bag deployment, dynamic stability control and rollover detection in automobiles, computer mice, pointers, video camera stabilization and a number of robotics and military applications. Conventional rotating wheel gyros and high precision fiber optic and ring laser gyros are too expensive and too large to be adopted into the market for micro gyroscopes. While potential markets for inexpensive gyroscopes exist, technical challenges have been impeding the rapid commercial deployment of gyroscopes.

The simplest alternative for low performance applications [3] is to obtain the angular velocity signal from two accelerometers separated by a distance 'b'. The average in output between the two accelerometers is a measure of linear acceleration (linear acc. = $(acc_1 + acc_2)/2$) and their difference is a measure of the angular acceleration (angular acc. = $(acc_1 - acc_2)/b$). Unfortunately, this method generates large errors since the angular velocity is the time integral of the linear acceleration. This means that special sensors for measuring angular velocity will always be needed. Note that linear acceleration cannot be derived from angular rate sensors in the way that angular velocity can be derived from accelerometers.

All reported micromachined gyroscopes [4] use vibrating mechanical elements to sense rotation. They have no rotating parts that require bearings and hence they can be easily miniaturized and batch fabricated using micromaching techniques. All vibratory gyroscopes are based on the transfer of energy between two vibration modes of a structure caused by Coriolis acceleration. Coriolis acceleration, named after the French scientist and engineer G.G. de Coriolis (1792-1843) is an apparent acceleration that arises in a rotating reference frame and is proportional to the rate of rotation.

1.2 Motivation

Gyroscopes are one of the biggest applications in the field of MEMS as accelerometers are implemented fairly well in commercial market. Some of the well known automotive applications are vehicle stability control, navigation assist, roll over detection are used in high end cars. Examples of consumer applications are 3D input devices, robotics, platform stability, camcorder stabilization, virtual reality etc.

Microgyroscopes are mainly attractive because of their small size (~ 1 mm X 1 mm including sensing circuits) and low cost. Most microgyroscopes consist of a vibrating proof-mass which is driven into oscillation by electrostatic or other means. When placed in a rotational field, the vibrating proof-mass experiences an apparent force called the Coriolis force, which is proportional to the cross-product of the angular velocity of the rotational field and the translational velocity of the oscillating proof-mass. The Coriolis force is orthogonal to the direction of the driven oscillation. The displacement induced by the Coriolis force is picked up by a sense accelerometer, which can either utilizing the vibrating proof-mass or have a separate sense proof-mass.

In the following analysis typical numbers for microgyroscopes are used in order to bring out the relative magnitudes of displacements and velocities in the driven (oscillation) direction and the induced (Coriolis force) direction. Typical values of the sense mass is about M_s = 1µg. The angular velocities that can be sensed are of the order of Ω = 1°/s. The oscillations are usually about 10 kHZ with an amplitude of about 5 µm. Therefore the peak oscillation velocity is about v_d = 0.31 m/s. The Coriolis force is then given by $Fc = 2\ M_s\Omega \times v_d$ = 10pN. Assuming a spring stiffness for the sense accelerometer of 1 (N/m), the sense displacement is about 10 pm. In any real microgyroscopes, some part of the driven oscillation couples onto the sense accelerometer, through electrostatic, inertial, viscous and

elastic modes. Comparing the magnitudes of the driven oscillation and the displacement produced by the sense accelerometer, it is seen that undesired coupling from the driven oscillation to the sense oscillation should be as small as 2 ppm. While this may be a difficult number to achieve in any low cost system, it is almost impossible to realize such precise dimension-control in IC-based processes which typically control relative fabrication tolerances to only about 1% or 10000 ppm. Furthermore, in capacitive sensors, a displacement of few picometers typically results in a capacitance change of a few zepto farads (10^{-21}). The total sense capacitance and parastic capacitances are usually of the order of ten to hundred femto farads, leading to a relative capacitance change of 0.1 ppm. Therefore, extremely low noise front ends are required to sense such small relative capacitance changes. Another fundamental issue which limits the resolution of microgyroscopes is mechanical thermal noise. Since IC processes and surface micromachining are both basically thin film processes, the resulting proof-masses tend to have a large surface area to volume ratio. As a result, viscous damping forces are more significant at the micro scale than at the macro scale. Therefore, the Brownian motion resulting from viscous loss mechanism sets a lower limit on the smallest deterministic motion that can be sensed.

1.3 Problem Statement

MEMS gyroscopes have proved to be extremely difficult to manufacture reliably. The MEMS gyroscope is required to sense picometer-scale displacements, making it sensitive to spurious vibrations and other coupling mechanisms. The difficulties of full time simulation of vibratory gyroscopes are often acknowledged. The major challenge simulating these systems is the existence of multiple time scales: one is defined by the natural frequency of the gyroscope (in kHZ range), the other – by the input angular velocity (ranging between degrees per second and sub-degrees per hour). These two time scales differ by more than 4-6 orders of magnitude. Straightforward plug-in of the equations of motion will simulate the behaviour of the system in the fastest time-scale. However, when the effects of

manufacturing defects or system response to control actions are examined, we are interested in the long-term behaviour of the system, which is of the order of the input angular velocity. Thus, direct substitution of governing equations into the simulation package is computationally impractical. This dissertation aims to study the behaviour of non-ideal vibratory gyroscopes, feasibility of adaptive mode tuning as an alternative to phase locked loop for mode matching and discuss the existing control strategies to behave close to the ideal gyroscope.

1.4 Outline of the dissertation

In this chapter, historical perspective of gyroscopes, problem statement and motivation for this dissertation is presented. In Chapter 2, fundamentals of micromachining are introduced. Emphasis is given on the major three techniques viz. Bulk micromachining, surface micromachining and the LIGA process. Also the advantages and application area of MEMS in various fields are brought out. Chapter 3 brings out the essential concepts of micromachined gyroscopes, classification of gyroscopes and the differential equations governing the ideal dynamical system. The methodology for simulation of errors particularly the anisoelasticity and anisodamping are discussed in Chapter 4. The existing control strategies for MEMS gyroscopes are brought out in Chapter 5. Control strategies proposed by Shkel et. al. in terms of quadrature controller, sliding mode controller proposed by Batur, the active disturbance rejection controller and adaptive mode tuning proposed by Leland are discussed. Results of simulation of ideal, non-ideal gyroscope with errors and adaptive mode tuning with linear phase detector and saturating phase detector with low pass filter are done with MATLAB/SIMULINK and its interpretation is given in Chapter 6. Finally the conclusion and future scope of MEMS gyroscope are in Chapter 7.

Fundamentals of Micromachining

2.1 Introduction

Microelectromechanical systems (MEMS) are small integrated devices or systems that combine electrical and mechanical components. They range in size from the sub micrometer (or sub micron) level to the millimeter level and there can be any number, from a few to millions, in a particular system. MEMS extend the fabrication techniques developed for the integrated circuit industry to add mechanical elements such as beams, gears, diaphragms, and springs to devices.

Examples of MEMS device applications include inkjet-printer cartridges, accelerometers, miniature robots, microengines, locks, inertial sensors, microtransmissions, micromirrors, micro actuators, optical scanners, fluid pumps, transducers, and chemical, pressure and flow sensors. New applications are emerging as the existing technology is applied to the miniaturization and integration of conventional devices.

These systems can sense, control, and activate mechanical processes on the micro scale, and function individually or in arrays to generate effects on the macro scale. The micro fabrication technology enables fabrication of large arrays of devices, which individually perform simple tasks, but in combination can accomplish complicated functions.

MEMS are not about any one application or device, nor are they defined by a single fabrication process or limited to a few materials. They are a fabrication approach that conveys the advantages of miniaturization, multiple components, and microelectronics to the design and construction of integrated electromechanical systems. MEMS are not only about miniaturization of

mechanical systems; they are also a new paradigm for designing mechanical devices and systems. Because of the significant impact that MEMS can have on the commercial and defense markets, industry and the government have both taken a special interest in their development.

2.2 Historical Background

The invention of the transistor at Bell Telephone Laboratories in 1947 sparked a fast-growing microelectronic technology. Jack Kilby of Texas Instruments built the first integrated circuit (IC) in 1958 using germanium (Ge) devices. It consisted of one transistor, three resistors and one capacitor. The IC was implemented on a slab of Ge that was glued on a glass slide. Later that same year Robert Noyce of Fairchild Semiconductor announced the development of a planar double-diffused Si IC. The complete transition from the original Ge transistors with grown and alloyed junctions to silicon (Si) planar double-diffused devices took about 10 years. The success of Si as an electronic material was due partly to its wide availability from silicon dioxide (SiO_2) (sand), resulting in potentially lower material costs relative to other semiconductors.

Since 1970, the complexity of ICs has doubled every two to three years. The minimum dimension of manufactured devices and ICs has decreased from 20 microns to the sub micron levels of today. Current ultra-large-scale-integration (ULSI) technology enables the fabrication of more than 10 million transistors and capacitors on a typical chip.

IC fabrication is dependent upon sensors to provide input from the surrounding environment, just as control systems need actuators (also referred to as transducers) in order to carry out their desired functions. Due to the availability of sand as a material, much effort was put into developing Si processing and characterization tools. These tools are now being used to advance transducer

technology. Today's IC technology far outstrips the original sensors and actuators in performance, size, and cost.

Attention in this area was first focused on microsensor (i.e., microfabricated sensor) development. The first microsensor, which has also been the most successful, was the Si pressure sensor. In 1954 it was discovered that the piezoresistive effect in Ge and Si had the potential to produce Ge and Si strain gauges with a gauge factor (i.e., instrument sensitivity) 10 to 20 times greater than those based on metal films. As a result, Si strain gauges began to be developed commercially in 1958. The first high-volume pressure sensor was marketed by National Semiconductor in 1974. This sensor included a temperature controller for constant-temperature operation. Improvements in this technology since then have included the utilization of ion implantation for improved control of the piezoresistor fabrication.

Around 1982, the term micromachining came into use to designate the fabrication of micromechanical parts (such as pressure-sensor diaphragms or accelerometer suspension beams) for Si microsensors. The micromechanical parts were fabricated by selectively etching areas of the Si substrate away in order to leave behind the desired geometries. Isotropic etching of Si was developed in the early 1960s for transistor fabrication. Anisotropic etching of Si then came about in 1967. Various etch-stop techniques were subsequently developed to provide further process flexibility.

These techniques also form the basis of the bulk micromachining processing techniques. Bulk micromachining designates the point at which the bulk of the Si substrate is etched away to leave behind the desired micromechanical elements. Bulk micromachining has remained a powerful technique for the fabrication of micromechanical elements. However, the need for flexibility in device design and performance improvement has motivated the development of new concepts and techniques for micromachining.

Among these is the sacrificial layer technique, first demonstrated in 1965 by Nathanson and Wickstrom, in which a layer of material is deposited between structural layers for mechanical separation and isolation. This layer is removed during the release etch to free the structural layers and to allow mechanical devices to move relative to the substrate. A layer is releasable when a sacrificial layer separates it from the substrate. The application of the sacrificial layer technique to micromachining in 1985 gave rise to surface micromachining, in which the Si substrate is primarily used as a mechanical support upon which the micromechanical elements are fabricated.

Prior to 1987, these micromechanical structures were limited in motion. During 1987-1988, a turning point was reached in micromachining when, for the first time, techniques for integrated fabrication of mechanisms (i.e. rigid bodies connected by joints for transmitting, controlling, or constraining relative movement) on Si were demonstrated. During a series of three separate workshops on microdynamics held in 1987, the term MEMS was coined. Equivalent terms for MEMS are microsystems (preferred in Europe) and micromachines (preferred in Japan).

2.3 Mechanical properties of Silicon

Silicon, an abundant material on earth, almost always exists in compounds with other elements [3]. Single-crystal silicon is the most widely used substrate material for MEMS and Microsystems. The popularity of silicon for such application is for the reasons below

(a) Silicon is mechanically stable and it can be integrated into electronics on the same substrate.

(b) Silicon is almost an ideal structural material. Materials with a high Young's modulus can better maintain a linear relationship between applied load and the induced deformations.

(c) Silicon has a melting point of 1400°C, which is twice as high as that of aluminium. This makes silicon dimensionally stable even at higher temperatures.

(d) Its thermal expansion coefficient is about 8 times smaller than that of steel and is more than 10 times smaller than that of aluminium.

(e) Silicon shows virtually no mechanical hysteresis. Thus it is an ideal candidate material for sensors and actuators. Silicon wafers are extremely flat and accept coatings and additional thin-film layers for building micro structural geometry or conducting electricity.

(f) Treatments and fabrication processes for silicon substrates are well established and documented.

2.4 Major branches of MEMS technology

Besides acceleration sensor and digital micro mirror, many new MEMS device categories were developed in the 1990s, with varying degrees of industrial implementation. A number of branches of MEMS have taken root and they are:-

(a) Optical MEMS. Monolithic integration of mechanics, electronics and optics using unique spatial or wavelength tenability resulting in improved efficiency of optical assembly and alignment accuracy. Typical examples are Micro machined optical switches for free-space optical interconnect

(b) BioMEMS. Miniaturisation (minimal invasion and size matched with biological entities) resulting in rich functional integration within physically small, minimally invasive medical devices. Examples include Micro structures and micro devices for retina implants, cochlear implants and sensor-enabled smart surgical work.

(c) RF MEMS. This promises direct integration of active and passive elements with circuitry resulting in unique performances not found in solid state RF integrated devices. Micro machined relays, tunable capacitors, micro integrated inductors and solenoid coils, etc are typical examples.

(d) Nano Electromechanical Systems (NEMS). The perceived driver of this technology is attributed to unique physical properties due to scaling (example ultra-low mass and ultra-high resonant frequency). This helps in unprecedented sensitivity and selectivity of detection achievable in selected classes. Typical examples include Nanotubes, chemical sensing and RF devices.

2.5 Microelectronics Vs MEMS

Technologies used in producing MEMS and Microsystems are inseparable from those of microelectronics. The boom of MEMS industry in the past decade is primarily due to the fact that microelectronics industry has matured considerably [3]. However, there are significant differences in the design and packaging of Microsystems from that of integrated circuits and microelectronics. The similarities and differences are as given in Table 2.5.1.

Microelectronics	**Microsystems (Silicon-based)**
Uses single crystal silicon die, silicon compounds and plastic	Uses single crystal silicon die and few other materials such as GaAs, quartz, polymers and metals.
Primarily 2-D structures	Complex 3-D structures
Stationary structures	May involve moving components
Fewer components in assembly	Many components to be assembled

Microelectronics	Microsystems (Silicon-based)
Transmits electricity for specific electrical functions	Performs a great variety of specific biological, chemical, electromechanical and optical functions
Complex patterns with high density over substrate	Simple patterns over substrates
IC die is completely protected from contacting media	Sensor die is interfaced with contacting media
Mature IC design technology	Lack of engineering design methodology and standards
Fabrication, manufacturing technology and packaging techniques are well established	Distinct manufacturing techniques and packaging technology is at infant stage

Table 2.5.1: Comparison of Microelectronics and Microsystems

2.6 Fabrication Technologies

The three characteristic features of MEMS fabrication technologies are miniaturization, multiplicity, and microelectronics. Miniaturization enables the production of compact, quick-response devices. Multiplicity refers to the batch fabrication inherent in semiconductor processing, which allows thousands or millions of components to be easily and concurrently fabricated. Microelectronics provides the intelligence to MEMS and allows the monolithic merger of sensors, actuators, and logic to build closed-loop feedback components and systems. The successful miniaturization and multiplicity of traditional electronics systems would not have been possible without IC fabrication technology. Therefore, IC fabrication technology, or microfabrication, has so far been the primary enabling technology for the development of MEMS. Microfabrication provides a powerful tool for batch processing and miniaturization of mechanical systems into a

technology for the development of MEMS. Microfabrication provides a powerful tool for batch processing and miniaturization of mechanical systems into a dimensional domain not accessible by conventional (machining) techniques. Furthermore, microfabrication provides an opportunity for integration of mechanical systems with electronics to develop high-performance closed-loop-controlled MEMS.

Advances in IC technology in the last few decades have brought about corresponding progress in MEMS fabrication processes. Manufacturing processes allow for the monolithic integration of microelectromechanical structures with driving, controlling, and signal-processing electronics. This integration promises to improve the performance of micromechanical devices as well as reduce the cost of manufacturing, packaging, and instrumenting these devices.

2.7 IC Fabrication

MEMS devices were first developed on silicon wafers because of the easy availability of mature processing technologies that had been developed with the microelectronics industry as well as the availability of expertise in process management and quality control.

Silicon actually comes in three general forms: single crystal silicon (SCS), poly crystalline silicon and amorphous silicon. In SCS material, the crystal lattice is regularly organised throughout the entire bulk. A poly crystalline silicon material is made of multiple crystalline domains. Within each individual domain, the crystal lattice is regularly aligned. However, crystal orientations are different in neighbouring domains. Amorphous silicon exhibits no crystalline regularilty.

Any discussion of MEMS requires a basic understanding of IC fabrication technology, or microfabrication, the primary enabling technology for the

development of MEMS. The major steps in IC fabrication technology are film growth, doping, lithography, etching, dicing, and packaging.

(a) Film growth: Usually, a polished Si wafer is used as the substrate, on which a thin film is grown. The film, which may be epitaxial Si, SiO_2, silicon nitride (Si_3N_4), polycrystalline silicon (polysilicon), or metal, is used to build both active or passive components and interconnections between circuits.

(b) Doping: To modulate the properties of the device layer, a low and controllable level of an atomic impurity may be introduced into the layer by thermal diffusion or ion implantation.

(c) Lithography: A pattern on a mask is then transferred to the film by means of a photosensitive (i.e., light sensitive) chemical known as a photoresist. The process of pattern generation and transfer is called photolithography. A typical mask consists of a glass plate coated with a patterned chromium (Cr) film.

(d) Etching: Next is the selective removal of unwanted regions of a film or substrate for pattern delineation. Wet chemical etching or dry etching may be used. Etch-mask materials are used at various stages in the removal process to selectively prevent those portions of the material from being etched. These materials include SiO_2, Si_3N_4 and hard-baked photoresist.

(e) Dicing: The finished wafer is sawed or machined into small squares, or dice, from which electronic components can be made.

(f) Packaging: The individual sections are then packaged, a process that involves physically locating, connecting, and protecting a device or component. MEMS design is strongly coupled to the packaging requirements, which in turn are dictated by the application environment.

2.8 Bulk Micromachining and Wafer Bonding

Bulk micro manufacturing involves the removal of materials from the bulk substrates, usually silicon wafers, to form the desired three-dimensional geometry of the microstructures. Shaping of micro system components of the size between 0.1 μm and 1 mm made of tough materials such as silicon is beyond any existing mechanical means. Physical or chemical techniques, either by dry or wet etching are the only the practical solutions. Orientation independent isotropic or anisotropic etching is the key technology used in bulk micro manufacturing.

Bulk micromachining is an extension of IC technology for the fabrication of 3D structures. Bulk micromachining of Si uses wet- and dry-etching techniques in conjunction with etch masks and etch stops to sculpt micromechanical devices from the Si substrate. The two key capabilities that make bulk micromachining a viable technology are:

(a) Anisotropic etchants of Si, such as ethylene-diamine and pyrocatechol (EDP), potassium hydroxide (KOH), and hydrazine (N_2H_4). These preferentially etch single crystal Si along given crystal planes.

(b) Etch masks and etch-stop techniques that can be used with Si anisotropic etchants to selectively prevent regions of Si from being etched. Good etch masks are provided by SiO_2 and Si_3N_4 and some metallic thin films such as Cr and Au.

A drawback of wet anisotropic etching is that the microstructure geometry is defined by the internal crystalline structure of the substrate. Consequently, fabricating multiple, interconnected micromechanical structures of free-form geometry is often difficult or impossible. Two additional processing techniques have extended the range of traditional bulk micromachining technology: deep anisotropic dry etching and wafer bonding. Reactive gas plasmas can perform

deep anisotropic dry etching of Si wafers, up to a depth of a few hundred microns, while maintaining smooth vertical sidewall profiles. The other technology, wafer bonding, permits a Si substrate to be attached to another substrate, typically Si or glass. Used in combination, anisotropic etching and wafer bonding techniques can construct 3D complex microstructures such as microvalves and micropumps.

The advantages and disadvantages of bulk micro manufacturing are:-

(a) Straightforward, involving well-documented fabrication processes.
(b) Less expensive, but material loss is high.
(c) Suitable for simple geometry.
(d) Limited to low-aspect ratio in geometry.

2.9 Surface Micromachining

Surface micro machining technique builds micro structure by adding materials layer by layer on top of the substrate. Deposition techniques, in particular the low pressure vapour deposition technique are used for such buildups. Polycrystalline silicon is the common layer material. Sacrificial layers, usually made of SiO_2, are used in constructing the MEMS components but are later removed to create necessary void space in the depth, i.e., in the thickness direction. Wet etching is the common method used for that purpose.

Surface micromachining enables the fabrication of complex multicomponent integrated micromechanical structures that would not be possible with traditional bulk micromachining. This technique encases specific structural parts of a device in layers of a sacrificial material during the fabrication process. The substrate wafer is used primarily as a mechanical support on which multiple alternating layers of structural and sacrificial material are deposited and patterned to realize micromechanical structures. The sacrificial material is then dissolved in a chemical etchant that does not attack the structural parts. The most widely used

surface micromachining technique, polysilicon surface micromachining, uses SiO_2 as the sacrificial material and polysilicon as the structural material.

At the University of Wisconsin at Madison, polysilicon surface micromachining research started in the early 1980s in an effort to create high-precision micro pressure sensors. The control of the internal stresses of a thin film is important for the fabrication of microelectromechanical structures. The microelectronic fabrication industry typically grows polysilicon, silicon nitride, and silicon dioxide films using recipes that minimize time. Unfortunately, a deposition process that is optimized to speed does not always create a low internal stress film. In fact, most of these films have internal stresses that are highly compressive (tending to contract). A freestanding plate of highly compressive polysilicon that is held at all its edges will buckle (i.e., collapse or give way). This is highly undesirable. The solution is to modify the film deposition process to control the internal stress by making it stress-free or slightly tensile.

One way to do this is to dope the film with boron, phosphorus, or arsenic. However, a doped polysilicon film is conductive, and this property may interfere with the mechanical devices incorporated electronics. Another problem with doped polysilicon is that it is roughened by hydrofluoric acid (HF), which is commonly used to free sections of the final mechanical device from the substrate. Rough polysilicon has different mechanical properties than smooth polysilicon. Therefore, the amount of roughening must be taken into account when designing the mechanical parts of the micro device.

A better way to control the stress in polysilicon is through post annealing, which involves the deposition of pure, fine-grained, compressive (i.e., can be compressed) polysilicon. Annealing the polysilicon after deposition at elevated temperatures can change the film to be stress-free or tensile. The annealing temperature sets the film's final stress. After this, electronics can then be

incorporated into polysilicon films through selective doping, and hydrofluoric acid will not change the mechanical properties of the material.

Deposition temperatures and the film's silicon to nitride ratio can control the stress of a silicon nitride Si_3N_4 film. The films can be deposited in compression, stress-free, or in tension.

Deposition temperature and post annealing can control silicon dioxide (SiO_2) film stress. Because it is difficult to control the stress of SiO_2 accurately, SiO_2 is typically not used as a mechanical material by itself, but as electronic isolation or as a sacrificial layer under polysilicon.

The advantages and disadvantages of surface micro machining are:-

(a) Requires the building of layers of materials on the substrate.
(b) Complex masking design and productions.
(c) Etching of sacrificial layers is necessary.
(d) Process is tedious and more expensive.
(e) Engineering problems such as interfacial stresses and stiction.
(f) Not constrained by the thickness of silicon wafers.
(g) Wide choices of film layers to be used.
(h) Suitable for complex geometries such as micro valves & actuators.

2.10 LIGA Process

LIGA process begins with deep X-ray lithography that sets the desired patterns on a thick film of photo resist. X-rays are used as the light source in photolithography because of their short wavelength, which provides higher penetration power into the photo resist materials. This high penetration power is necessary for high resolution in lithography and for a high aspect ratio in the depth. The major fabrication steps in the LIGA process is shown in Fig 2.10.1.

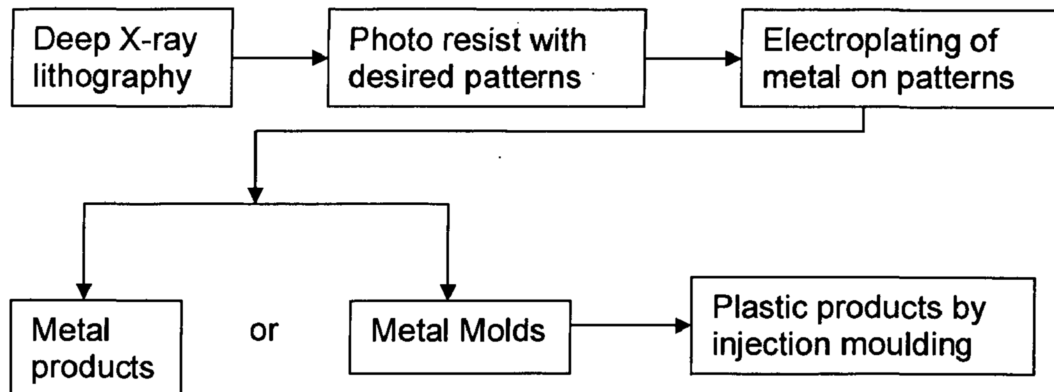

Fig 2.10.1 Fabrication steps in the LIGA process

The merits and demerits of LIGA process are

(a) The most expensive process.

(b) Requires a special synchrotron radiation facility for deep x-ray lithography

(c) Requires development of microinjection molding technology and a facility for mass production processes.

(d) Virtually unlimited aspect ratio of microstructure geometry.

(e) Flexible microstructure configurations and geometry.

(f) Technique allows production of metallic microstructures.

(g) Best manufacturing process for mass production.

(h) Requires a special synchrotron radiation facility for deep x-ray lithography

(e) Requires development of microinjection molding technology and a facility for mass production processes.

(f) Virtually unlimited aspect ratio of microstructure geometry.

(g) Flexible microstructure configurations and geometry.

(h) Technique allows production of metallic microstructures.

(i) Best manufacturing process for mass production.

2.11 Advantages of MEMS

The ability to seamlessly integrate mechanical sensors and actuators with electronic processors and controllers at the chip level is unique of MEMS. MEMS technology can realize two or three dimensional features with small dimensions and precision that cannot be reproducible, efficient or profitable with traditional machining tools. Combined with photolithography, MEMS technology can realize unique three-dimensional features, such as inverted pyramid cavities, high aspect ratio trenches, through wafer holes, cantilevers and membranes.

2.12 Applications of MEMS

Some examples of application of MEMS technology are in:

(a) Pressure and Inertial Sensors.

(b) Accelerometers and Gyroscopes.

(c) Printers, automobiles, and biomedical diagnostic equipment

(d) Microengines.

(e) Microtransmissions using sets of small and large gears interlocking with other sets of gears to transfer power.

(f) A micro-optoelectromechanical system device for fiber cross-connect.

(g) Fabricating vaporization microchambers for vaporizing liquid microthrusters for nanosatellites

2.13 The Future of MEMS

Each of the three basic microsystems technology processes we have seen, bulk micromachining, sacrificial surface micromachining, and micromolding/LIGA, employs a different set of capital and intellectual resources. MEMS technology has the potential to change our daily lives as much as the computer has.

However, the material needs of the MEMS field are at a preliminary stage. A thorough understanding of the properties of existing MEMS materials is just as important as the development of new MEMS materials.

Future MEMS applications will be driven by processes enabling greater functionality through higher levels of electronic-mechanical integration and greater numbers of mechanical components working alone or together to enable a complex action. Future MEMS products will demand higher levels of electrical-mechanical integration and more intimate interaction with the physical world.

Basics of MEMS Gyroscopes

Fabrication technologies [6] for microcomponents, microsensors, micromachines and microelectromechanical systems (MEMS) are being rapidly developed, and represent a major research effort worldwide. Many techniques are being utilized in production of different types of MEMS, including inertial microsensors, which have made it possible to fabricate MEMS in high volumes at low individual cost. Micromechanical vibratory gyroscopes or angular rate sensors have a large potential for different types of applications as primary information sensors for guidance, control and navigation systems. They represent an important inertial technology because other gyroscopes such as solid-state gyroscopes, laser ring gyroscopes, and fiber optic gyroscopes, do not allow for significant miniaturization.

There is considerable difficulty in producing micro sized bearings; all micro gyroscopes indeed work on vibrational principles. Vibratory gyroscopes work on the principle of conservation of momentum. The gyroscopes sense the transfer of motion from one vibrational mode to a second due to rotation induced Coriolis force coupling.

3.1 Operation principle

In most micromechanical vibratory gyroscopes, the sensitive element can be represented as an inertia element and elastic suspension with two prevalent degrees of freedom (see figure 3.1)

Massive inertia element is called proof mass. The sensitive element is driven to oscillate at one of its modes with prescribed amplitude. This mode usually is called primary mode. When the sensitive element rotates about a particular fixed-body axis, which is called sensitive axis, the resulting Coriolis force causes the

proof mass to move in a different mode. Information about external angular rate is contained in these different oscillations.

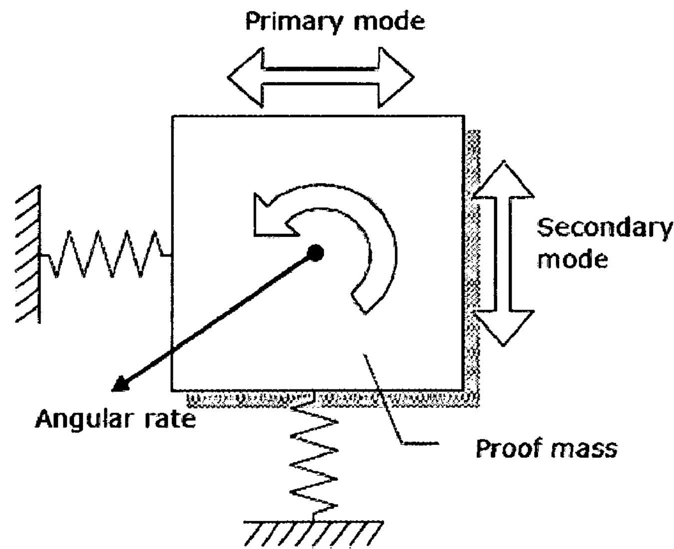

Fig 3.1 Operation principle. Courtesy www.astrise.com

3.2 Classification of gyroscopes

With respect to the number of inertia elements used, the nature of primary and secondary motions of the sensitive element, classification of the vibratory gyroscopes can be represented as shown in figure 3.2.

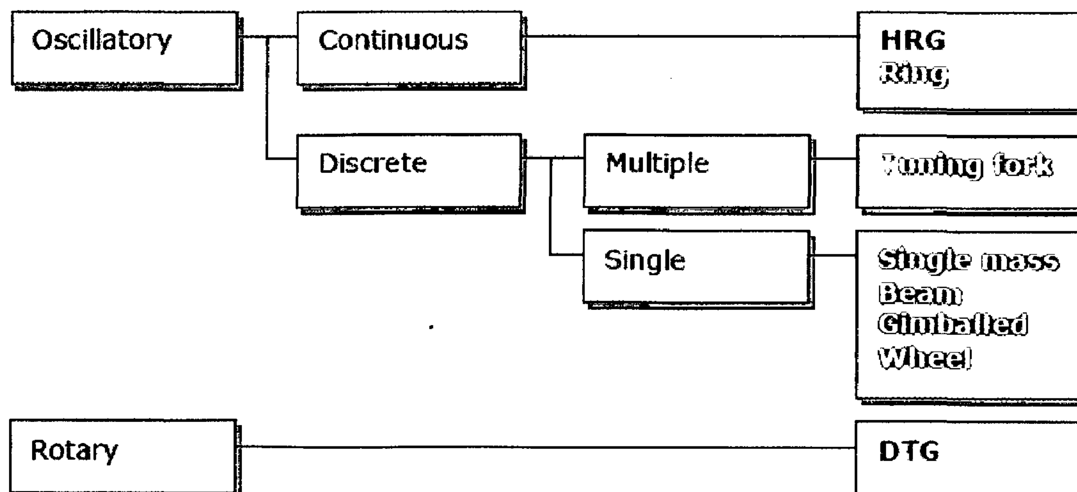

Fig 3.2 Classification of the vibratory gyroscopes

Single degree of freedom gyroscopes [1] mentioned above can be of two t viz. rate gyro and rate integrating gyro. Rate gyro, an open loop sensor, provides a signal proportional to the rate of rotation (angular velocity). It is cheaper to implement and hence costs less. The rate integrating gyro, a closed loop sensor, will be directly measuring the absolute angle of the object. Since it is closed loop, the measurement values have higher accuracy.

Gyroscopes can be classified into three different categories [4] based on their performance: inertial grade, tactical grade and rate grade devices. From the late 1990s, much of the effort in developing micromachined silicon gyroscopes has concentrated on "rate-grade" devices, primarily because of their use in automotive applications. There are also several other applications that require improved performance, including inertial navigation, guidance, robotics and some consumer electronics. Table 3.2.1 summarises the requirements for each of these categories.

Parameter	Rate Grade	Tactical Grade	Inertial Grade
Angle Random Walk, $°/\sqrt{h}$	>0.5	0.5-0.05	<0.001
Bias Drift, $°/\sqrt{h}$	10-1000	0.1-10	<0.01
Scale Factor Accuracy, %	0.1-1	0.01-0.1	<0.001
Full Scale Range (°/sec)	50-1000	>500	>400
Max. shock in 1msec, g's	10^3	10^3-10^4	10^3
Bandwidth, Hz	>70	~100	~100

Table 3.2.1 Performance requirements for different classes of Gyroscopes

3.3 Ideal dynamical system

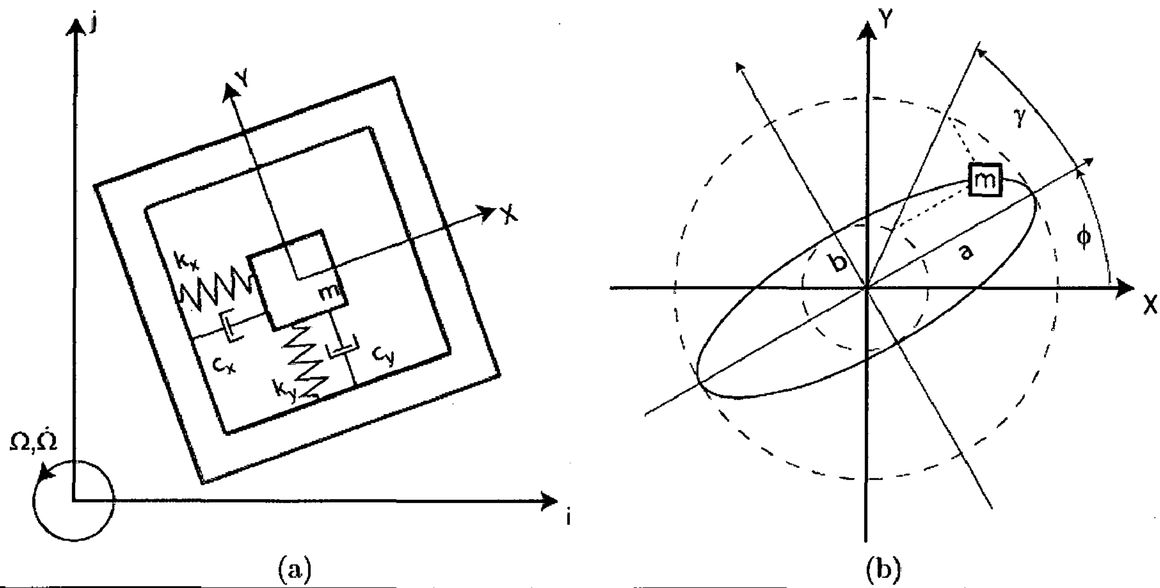

Fig 3.3 (a) Dynamic system for rate integrating gyroscope. (b) Trajectory of the vibrating mass in terms of the orbital elements.

Consider a mass-spring system with a moving **X-Y** coordinate system with respect to an **i-j** fixed world frame (Fig 3.3(a)). The position p of the mass m at a given time t in the moving co-ordinate system is

$$p = (x)\mathbf{X} + (y)\mathbf{Y} \tag{3.3.1}$$

The velocity **v** of the mass as induced by the rotation is then given by

$$\mathbf{v} = \frac{d\mathbf{p}}{dt} + (\Omega \mathbf{p}) \tag{3.3.2}$$

$$\mathbf{v} = (\dot{x} - \Omega y)\mathbf{X} + (\dot{y} + \Omega x)\mathbf{Y} \tag{3.3.3}$$

The induced acceleration a is then

$$a = \frac{d\mathbf{v}}{dt} + (\Omega \mathbf{v}) \tag{3.3.4}$$

$$a = (\ddot{x} - \Omega^2 x - 2\Omega\dot{y} - \dot{\Omega}y)\mathbf{X} + (\ddot{y} - \Omega^2 y + 2\Omega\dot{x} + \dot{\Omega}x)\mathbf{Y} \tag{3.3.5}$$

From Newton's second law, the equations of motion are of the mass-spring-damper system with respect to the moving coordinate system are

$$\begin{aligned} ma_x + c_x\dot{x} + k_x x = 0 \\ ma_y + c_y\dot{y} + k_y y = 0 \end{aligned} \qquad (3.3.6)$$

Where a_x and a_y, k_x and k_y, c_x and c_y are the x and y components of **a**, stiffness, and damping respectively. Substituting the values from (3.3.5) gives

$$\begin{aligned} m\ddot{x} + c_x\dot{x} - 2m\Omega\dot{y} + (k_x - m\Omega^2)x - m\dot{\Omega}y = 0 \\ m\ddot{y} + c_y\dot{y} + 2m\Omega\dot{x} + (k_y - m\Omega^2)y + m\dot{\Omega}x = 0 \end{aligned} \qquad (3.3.7)$$

In an ideal implementation of the gyroscope, the rotation is constant ($\dot{\Omega} = 0$), the stiffness values are equal and are much larger than the mass times the rotation squared ($k = k_x = k_y$, $k >> m\Omega^2$), and in this discussion, damping is neglected (c_x and $c_y \approx 0$). This damping assumption can be justified by the fact a control will be implemented to compensate for energy losses. With these simplifications and dividing by mass, the equations of motion become,

$$\begin{aligned} \ddot{x} + \omega_n^2 x - 2\Omega\dot{y} = 0 \\ \ddot{y} + \omega_n^2 y + 2\Omega\dot{x} = 0 \end{aligned} \qquad (3.3.8)$$

where $\omega_n = \sqrt{k/m}$ is the natural frequency. In a non-rotating system (Ω=0), the solution is an ellipse of semi-major axis length a, semi-minor axis length b, and oriented at an angle Φ from the X-Y axes (Fig 3.3(b)). A convenient way of expressing the dynamics of the system is using these elliptical "orbital" variables as proposed by Friedland and Hutton [7]. When the ellipse is oriented with the X-Y axes, the solution can be expressed by

$$x = a\cos(\omega_n t + \gamma_0) \qquad (3.3.9)$$

$$y = b\cos(\omega_n t + \gamma_0) \qquad (3.3.10)$$

Where γ_0 defines the initial "orbital angle" γ which designates the starting point of the mass on the ellipse. To account for the orientation of the ellipse, we use a

coordinate transform by a rotation ϕ. The complete generalized elliptical equations are then

$$x = a\cos\phi\cos(\omega_n t + \gamma_0) - b\sin\phi\sin(\omega_n t + \gamma_0) \tag{3.3.11}$$

$$y = a\sin\phi\cos(\omega_n t + \gamma_0) + b\cos\phi\sin(\omega_n t + \gamma_0) \tag{3.3.12}$$

Based on the position and velocity, the orientation angle can be instantly calculated by

$$\tan 2\phi = \frac{2(\omega_n^2 xy + \dot{x}\dot{y})}{\omega_n^2(x^2 - y^2) + (\dot{x}^2 - \dot{y}^2)} \tag{3.3.13}$$

Now, factoring in the rotation of the system ($\Omega \neq 0$) adds an additional degree of complexity to the problem. However, while x and y are changing very quickly over one period of vibration, the orbital parameters, a, b and ϕ remain nearly constant over one period. Thus averaging techniques may be implemented to approximate the long term behaviour of the slowly varying orbital parameters. Friedland and Hutton [7] solved this problem under the assumption that the ellipse is intentionally kept very thin (b=0) in order to reduce the effects of anisoelasticity. The approximate long term behaviour under these assumptions is the solution of the orbital element state equations

$$\dot{a} = 0 \tag{3.3.14}$$

$$\dot{b} = 0 \tag{3.3.15}$$

$$\dot{\phi} = -\Omega \tag{3.3.16}$$

$$\dot{\theta} = \omega \tag{3.3.17}$$

Thus we see that when the device is rotated at a constant velocity Ω, the vibration pattern will precess with the same angular velocity, but in the opposite direction with respect to a viewer in the moving frame. Assuming the oscillation pattern initially coincides with the X-Y coordinate system (ϕ = 0), the inclination of the ellipse ϕ, which can be found at any given time by (3.3.13), is exactly equal to the angle of rotation of the device

$$\phi = \int_0^t \Omega dt \tag{3.3.18}$$

Thus a device operating on this principle mechanically integrates any input angular rate and an output angular displacement. This can be resolved without integrating any electronic signals. An important property is that even if Ω varies in time, equation (3.3.18) is still valid. Since (3.3.18) is twice differentiable, it can be observed that the angular acceleration $\dot{\Omega}$ of the wave precession is equal to the negative angular acceleration of the device. Thus the calculated precession angle is invariant to changes in the angular rate.

3.4 Mode matching

Most of the reported micromachined vibratory rate gyroscopes have a single proof mass suspended above the substrate. The proof mass is supported by anchored flexures, which serve as the flexible suspension between the proof mass and the substrate, making the mass free to oscillate in two orthogonal directions – the drive and the sense.

The proof mass is driven into resonance in the drive direction by an external sinusoidal force. When the gyroscope is subjected to an angular rotation, the Coriolis force is induced in the y-direction. If the drive and sense resonant frequencies are matched, the Coriolis force excites the system into resonance in the sense direction. The resulting oscillation amplitude in the sense direction is proportional to the Coriolis force, and thus, to the angular velocity to be measured. The sense direction oscillation is detected generally by air-gap capacitors.

To achieve the maximum possible gain, the conventional gyroscopes are generally designed to operate at or near the peak of the response curve. This is typically achieved by matching drive and sense resonant frequencies. However, the system becomes very sensitive to variations in system parameters causing a shift in the resonant frequency.

Under high quality factor conditions the gain is high, however the bandwidth extremely narrow. For example, 1% fluctuation in frequency matching between drive and sense modes will produce an error of 20% in the output signal gain depending on the damping conditions. In addition, the gain is affected significantly by fluctuations in damping.

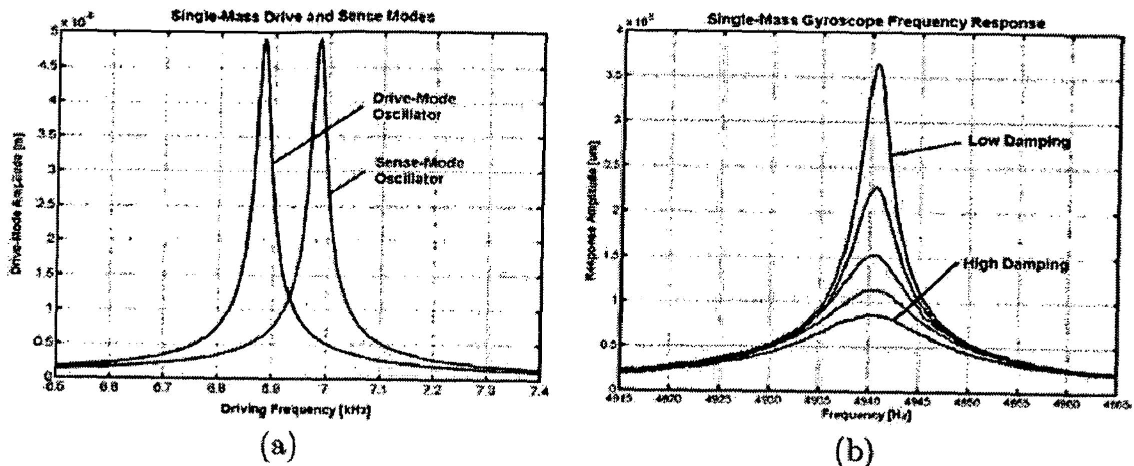

Figure 3.4(a) Driving frequency (in KHz) versus Drive Mode amplitude (in m).
Figure 3.4(b) Frequency (in Hz) versus Response Amplitude (in μm)
Figures obtained from [17]

Theory of Adaptive Mode Tuning is discussed in Chapter 5 which does not utilize the conventional phase locked loop and uses adaptive control.

Simulation of errors in Micromachined Gyroscopes

4.1 Introduction

Difficulties of full-time scale simulation of vibratory gyroscopes are often acknowledged [8]. The major challenge simulating these systems is the existence of multiple time-scales: one is defined by the natural frequency of the gyroscope (in KHz range), the other – by the input angular velocity (ranging between degrees per second and sub-degrees per hour). These two time scales differ by more than 4-6 orders of magnitude. Straightforward plug-in of the equations of motion into one of the numerical integration packages will simulate the behaviour of the system in the fastest time-scale. However, when the effects of manufacturing defects or system response to control actions are examined, we are interested in the long term behaviour of the system, which is of the order of the input angular velocity. Thus, direct substitution of governing equations into the simulation package is computationally impractical.

Fabrication of micromachined gyroscopes involves multiple processing steps including the deposition, etching and patterning of materials. Depending on the technology, different number of steps is involved and different fabrication tolerances can be achieved at each step. As a rule, every fabrication step contributes to imperfections in the gyroscope. Understanding of the behaviour of gyroscopes in presence of imperfections and ability to control and compensate for defects are essential for improving its performance. All micromachined gyroscopes are planar vibratory mechanical structures fabricated primarily from polysilicon or single crystal silicon. In practice, imperfections are reflected in asymmetry and anisoleasticity of the structure. Consequently, asymmetries result in undesirable constantly acting perturbations in the form of mechanical and electrostatic forces.

4.2 Modeling of imperfections

The governing equations in Cartesian coordinates of a non-ideal gyroscope are given by

$$\begin{aligned} \ddot{X} + \omega_n^2 X - 2\Omega\dot{Y} &= (\omega_n^2 - \omega_x^2)X + C_{xy}Y + D_{xx}\dot{X} + D_{xy}\dot{Y} \\ \ddot{Y} + \omega_n^2 Y + 2\Omega\dot{X} &= (\omega_n^2 - \omega_y^2)X + C_{yx}X + D_{yy}\dot{Y} + D_{yx}\dot{X} \end{aligned} \tag{4.2.1}$$

The terms on the right hand side represent potential sources of error which can be viewed as external perturbations of the ideal system. The coefficients multiplying the position variables represent non-ideal spring forces that could arise, for example from the lack of perfect symmetry in the device. They may be collectively identified as "anisoelasticity". The terms multiplying the velocity variables are damping terms and could represent losses in the system due to various physical causes such as structural damping, transmission of energy to suspension, etc.

Two types of error signals arise in the sense output due to non-Coriolis induced coupling: non proportional damping leads to errors in phase and anisoleastic effects lead to errors in quadrature with the Coriolis-force-induced displacement. Anisoleasticity denotes the angular mismatch between the measurement coordinates and the principal stiffness axes and non proportional damping signifies that the damping matrix is not proportional to either stiffness and/or mass matrix.

Accurate modeling and identification of coupling due to elastic and dissipative forces will significantly enhance the ability to compensate for the consequent errors via feedback/feed forward control strategies – thus leading to the next generation "smart" MEMS gyroscopes with self-calibrating capabilities. The left hand side of the governing equations (4.2.1) models an ideal vibratory gyroscope with matched natural frequencies ω_n. The essential feature of these equations is the presence of the Coriolis acceleration terms $-2\Omega\dot{Y}$ and $2\Omega\dot{X}$. These two terms

will appear only if the equations of motion are written in a non-inertial coordinate frame. It is the Coriolis acceleration that causes a transfer of energy between two of the gyros modes of operation.

For any two dimensional system of springs, no matter how complex, one can uniquely define two principal spring axes (or main axes of elasticity) and corresponding equivalent spring constants. In the ideal gyroscope, the principal axes of elasticity have equal stiffness and coincide with the x-y coordinate system (Fig 4.2.1). In the presence of imperfections, there is a mismatch in the principal stiffness values, $2h = (K_1\text{-}K_2)$ and an angular mismatch of the principal axes from the x-y coordinate system by an angle α (Fig 4.2.2)

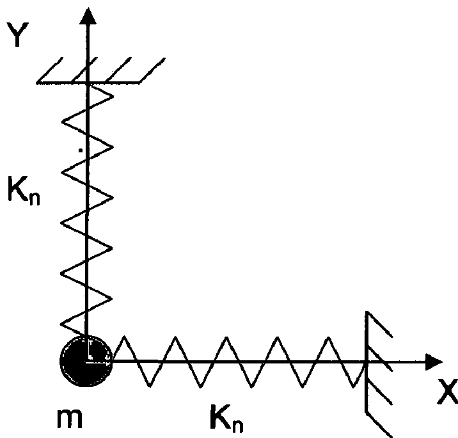

Fig 4.2.1 Ideal gyroscope

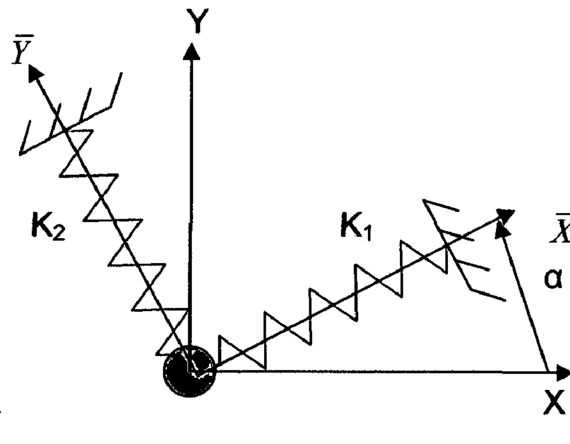

Fig 4.2.2 Anisoelasticity in gyroscope

To a first order approximation, the non-ideal dynamical system in matrix form as

$$\begin{bmatrix} m & 0 \\ 0 & m \end{bmatrix}\begin{pmatrix} \ddot{x} \\ \ddot{y} \end{pmatrix} + \begin{bmatrix} C_{xx} & C_{xy} - 2m\Omega \\ -C_{yx} + 2m\Omega & C_{yy} \end{bmatrix}\begin{pmatrix} \dot{x} \\ \dot{y} \end{pmatrix} + \begin{pmatrix} K_{xx} & K_{xy} \\ K_{yx} & K_{yy} \end{pmatrix}\begin{pmatrix} x \\ y \end{pmatrix} = \begin{pmatrix} F_x \\ F_y \end{pmatrix} \tag{4.2.2}$$

where m is the lumped mass approximation for the gyroscope, K_{xx}, K_{xy}, K_{yx},and K_{yy} are the non-ideal stiffness terms, C_{xx}, C_{xy}, C_{xy} and C_{yy} are the non-ideal damping terms and F_x and F_y are applied forces. Non-idealities that vary with position and velocity can also be referred as anisoelasticity and anisodamping.

The off diagonal elements in the stiffness matrix appear when the main axes of elasticity do not coincide with the coordinate system {x y}. By analogy with stiffness, damping can also be described in terms of two main axes of damping. In general, the principal axes of elasticity and damping are not necessarily aligned because asymmetry in stiffness and damping are caused by different physical phenomena. Thus, off-diagonal elements in the damping matrix also appear due to misalignment of the main axes of damping with the coordinate axes {x y}.

4.3 Off-diagonal elements

If the "input" angular velocity Ω is zero, and under certain appropriate initial conditions, the ideal gyroscope will oscillate along a straight line. The orientation of the straight line is defined by initial conditions. In a more general case, when the initial conditions are such that the vector of displacement is not parallel to the vector of velocity, the "orbit" of the gyroscope motion is an ellipse. Thus the ideal system is supposed to oscillate along a horizontal straight line with constant amplitude and frequency. Off diagonal elements in the stiffness matrix result in frequency change and disruption of the straight line oscillation. Off-diagonal symmetric elements in the damping matrix result in precession of the straight line oscillation and amplitude change.

On the other hand, skew-symmetric terms in the damping matrix cause only precession of the gyroscope line of oscillation. The effect of off-diagonal elements is not distinguishable from the effect of the Coriolis force, and thus present significant difficulties for their compensation. Perturbations proportional to the velocity can appear as a result of losses due to structural damping, transmission of energy to suspension, aerodynamic drag, etc. Gyroscopic forces (skew-symmetric terms in damping matrix) can appear only as inertial forces or as a side effect of an active control.

4.4 Analysis of imperfections

Analysis of gyroscopes in presence of these imperfections does not require any special treatment and can be done using the eigenvalue analysis. When there is no input rotation and only anisoelasticity is present, the equations of motion have the form

$$\begin{bmatrix} \ddot{X} \\ \ddot{Y} \end{bmatrix} + \begin{bmatrix} \omega_n^2 & C_{xy} \\ C_{xy} & \omega_n^2 \end{bmatrix} \begin{bmatrix} X \\ Y \end{bmatrix} = 0 \qquad (4.4.1)$$

The eigen vectors of this system define a pair of principal (cardinal) elastic axes that define stable directions of a straight line motion of the gyroscope. Assume that the axes of symmetry of the ideal (defect free) gyroscope are X and Y (refer Figure 4.2.1). Due to imperfections in the fabrication the X and Y axes may not coincide with the principal axes of elasticity $\bar{X}$ and $\bar{Y}$. Then the stiffness matrix in {X Y} coordinate frame has the form

$$K = \begin{bmatrix} K_{xx} & K_{xy} \\ K_{yx} & K_{yy} \end{bmatrix}, \; K_{xy} = K_{yx} \qquad (4.4.2)$$

Assume that the principal spring axes are titled by an angle α from the reference coordinate system (Figure 4.2.2). Also assume that the principal spring constants are K_1 and K_2 ($K_1 > K_2$). Then elements of the stiffness matrix can be presented in terms of K_1, K_2 and α as follows:

$$\begin{aligned} K_{xx} &= \frac{K_1 + K_2}{2} + \frac{K_1 - K_2}{2}\cos(2\alpha) \\ K_{yy=} &= \frac{K_1 + K_2}{2} + \frac{K_2 - K_1}{2}\cos(2\alpha) \\ K_{xy} = K_{yx} &= \frac{K_1 - K_2}{2}\sin(2\alpha) \end{aligned} \qquad (4.4.3)$$

By analogy with stiffness, damping can also be described in terms of two main axes of damping. In general, the principal axes of elasticity and damping are not necessarily aligned because asymmetry in stiffness and damping are caused by different physical phenomena. The location of the principal axis of damping and magnitude of the damping difference are determined by an averaging of the

damping asymmetries. By analogy with stiffness, damping matrix D can be written as a function of principal damping constants, D_1, D_2 and the angle of axes orientation β. It has the form

$$\begin{bmatrix} \frac{D_1+D_2}{2}+\frac{D_1-D_2}{2}\cos(2\beta) & \frac{D_1-D_2}{2}\sin(2\beta) \\ \frac{D_1-D_2}{2}\sin(2\beta) & \frac{D_1+D_2}{2}+\frac{D_2-D_1}{2}\cos(2\beta) \end{bmatrix} \quad (4.4.4)$$

Damping asymmetry, like damping itself, arises principally from asymmetry in aerodynamic drag, structural damping, and transmission of energy to the suspension etc. Major damping mechanisms involved in the vibratory gyroscope include viscous damping of the ambient air and the air layer between the proof mass and the substrate [9].

4.5 Motion decomposition

The application of the method of motion decomposition consists of the following steps. First we introduce the characteristic parameters of the system. This is followed by a non-dimensional analysis with respect to the chosen time-scale and identification of the small parameters of the system. The decomposition procedure is concluded by the averaging of the system with respect to the time scale of interest. The application of this method to vibratory gyroscopes allows rapid simulation of the long-term response of the gyroscopes to the constantly acting perturbations. Details of the procedure can be found in [10].

The equations of motion with perturbations in non-dimensional form:

$$\begin{aligned} \ddot{x}_1 + x_1 &= \alpha Q_1(t,x,\dot{x}) \\ \ddot{x}_2 + x_2 &= \alpha Q_2(t,x,\dot{x}) \\ \alpha &\approx \frac{\Omega}{\omega_n} << 1 \end{aligned} \quad (4.5.1)$$

Here $x=(x_1,x_2)$ is a non-dimensional displacement, Q_1 and Q_2 are constantly acting perturbations including the Coriolis force, α is a small non-dimensional parameter defined by characteristic values of the system.

The first step of the procedure is to find a non-perturbed solution of the system (4.5.1), i.e. when α=0. In this case, the solution is

$$\begin{aligned} x_1 &= C_1 \cos t + C_3 \sin t \\ \dot{x}_1 &= -C_1 \sin t + C_3 \cos t \\ x_2 &= C_2 \cos t + C_4 \sin t \\ \dot{x}_2 &= -C_2 \sin t + C_4 \cos t \end{aligned} \qquad (4.5.2)$$

The second step is to define a coordinate transformation $x(t) = g(t, y(t))$ which has a topology (4.5.2) of the non-perturbed system (4.5.1)

$$\begin{aligned} x_1 &= y_1 \cos t + y_3 \sin t \\ \dot{x}_1 &= -y_1 \sin t + y_3 \cos t \\ x_2 &= y_2 \cos t + y_4 \sin t \\ \dot{x}_2 &= -y_2 \sin t + y_4 \cos t \end{aligned} \qquad (4.5.3)$$

The transformation (4.5.3) will result in the system of the standard form

$$\frac{dy}{dt} = \alpha Y(y,t) \qquad (4.5.4)$$

where y = (y_1, y_2, y_3, y_4) and

$$Y(y,t) = J^{-1} Q(q(t,y)) = \begin{bmatrix} -\sin t & 0 \\ 0 & -\sin t \\ \cos t & 0 \\ 0 & \cos t \end{bmatrix} \begin{bmatrix} Q_1 \\ Q_2 \end{bmatrix} \qquad (4.5.5)$$

Here J^{-1} is the inverse of the Jacobian of the transformation $x(t) = g(t, y(t))$. The right hand side of (4.5.4) is an explicit function of the state vector y and time t. Since the solution (4.5.2) of the non-perturbed equation (4.5.1) is periodic, time averaging can be applied. This results in a simplified equation:

$$\frac{dy}{dt} = \alpha \overline{Y}(y) \qquad (4.5.6)$$

where

$$\overline{Y}(y) = \frac{1}{2\pi} \int_0^{2\pi} Y(y,t) dt$$

The procedure described in this section, transforms the original system into the normalized system (4.5.1), which after averaging is transformed to (4.5.6). The underlying theory of this method guarantees that the solution of the system

(4.5.6) is close to the solution of (4.5.1). The new system (4.5.6) allows fast simulation of the long term response (in the time scale of the input angular velocity) of the non-ideal gyroscope.

The decomposition procedure described in this section makes the simulation of the long-term behaviour of the gyroscope in presence of perturbations very computationally efficient. In the next section, we classify errors in vibratory gyroscopes based on the results of motion decomposition.

4.6 Classification of errors.

Nominally, the gyroscope oscillates along the x-axis. If there is no anisoelasticity present (i.e.) stiffness matrix is diagonal, it causes only frequency change though the line of oscillation remains the same. The hyperbolic potential forces (positive definite stiffness matrix) in addition to the frequency changes result in a disruption of the straight line oscillation. Non-potential forces can appear only if off-diagonal elements in the stiffness matrix are not equal. They can appear as a side effect of the active control. These forces also cause disruption of the straight line oscillation but do not result in frequency change.

Asymmetry in damping can be presented in the form of dissipative spherical forces, dissipative hyperbolic forces and gyroscopic forces. The dissipative spherical forces cause only amplitude changes. Hyperbolic velocity dependent forces result in precession of the straight line oscillation and amplitude change. Gyroscopic forces can cause only precession. Dissipative spherical forces and hyperbolic forces can appear as a result of losses due to structural damping, transmission of energy to suspension, aerodynamic drag etc. Gyroscopic forces can appear only as inertial forces or as a side effect of the active control.

The most dangerous perturbations for the gyroscope operation are hyperbolic potential forces, non-potential forces, hyperbolic velocity dependent forces and gyroscopic-like forces appearing as off-diagonal elements in the damping matrix.

All the above said errors are simulated using MATLAB/SIMULINK package and the results are discussed in Chapter 6.

Control Strategies for Micromachined Gyroscopes

5.1 Introduction

Micromachined gyroscopes typically rely on the coupling of an excited vibration mode into a secondary mode due to the Coriolis acceleration. The magnitude of oscillation in the sense mode provides a measure of the input angular velocity. These devices require no rotational parts which would need bearings and hence can be relatively easily miniaturized. The sensing element must be able to move and hence can be controlled in two degrees of freedom, one for the excited or driven mode, the other for the sense mode. One way of describing a micromachined gyroscope is that it acts as a resonator in the drive direction and as an accelerometer in the sense direction. Since the Coriolis acceleration is proportional to the velocity of the driven mode, it is desirable to make the amplitude and the frequency of the drive oscillation as large as possible. At the same time it has to be ensured that the frequency and amplitude remain constant since even very small variations can swamp the Coriolis acceleration. For amplitude control typically an automatic gain control loop is used, frequency stability can be ensured by a phase locked loop.

Vibratory gyroscopes [4] can be operated open or closed loop to measure rate of rotation (angular velocity). In the open loop mode, the response to a change in rotation is not instantaneous, as time is required for the amplitude of the sense mode to reach its steady-state value. In the closed loop mode of operation, the sense mode amplitude is continuously monitored and driven to zero and hence the bandwidth and dynamic range of the sensor can be increased beyond the open-loop values even with matched resonant modes. The bandwidth is then limited by the readout and control electronics and can be increased to values approaching the resonant frequency of the structure.

Most MEMS gyroscopes [15] are operated in the open loop mode. The main advantage of open loop mode of operation is that circuitry used for the operation of gyroscope in this mode is simpler than in the other modes, since there is no control action in the sense axis. However, under an open loop mode of operation, the gyroscope's angular rate scale factor is very sensitive and not constant over any appreciable bandwidth to fabrication defects and environment variation. Therefore, the application areas for the open loop mode are limited to those which require low cost and low performance gyroscopes.

In contrast to the open loop mode of operation, in the closed loop mode of operation, the sense amplitude of oscillation is continuously monitored and driven to zero. As a consequence, the bandwidth and dynamic range of the gyroscope can be greatly increased beyond what can be achieved with the open loop mode of operation. However, under conventional closed loop mode of operation, it is difficult to ensure a constant noise performance, in the face of environment variations such as temperature changes, unless an on line mode tuning scheme is included. Moreover, there are practical difficulties in designing a feedback controller so that the closed loop system is stable and sufficiently robust for gyroscopes with high Q systems. Therefore the application areas for the conventional closed loop mode of operation are those which require medium cost and medium performance gyroscopes.

5.2 Quadrature control

In this case, the gyroscope control system [12] performs four basic tasks:

(a) Initiates oscillation until the appropriate energy level is reached.

(b) Maintains the reached energy level.

(c) Compensates for quadrature deviation from the reference straight line of oscillations.

(d) Senses displacements and velocities in orthogonal directions.

Traditionally tasks (a) and (b) are solved by driving a micro-machined structure at resonance. This is typically done by employing a transresistance amplifier configured in positive feedback. The oscillation amplitude can be kept constant using an automatic gain control loop. The task (d) can be solved using lateral and differential comb fingers. The lateral interdigitated comb fingers can be used to measure linear velocity of the proof-mass and parallel plate capacitive arrangements can be used to measure deflection of the structure. Practical examples of arrangements are reviewed in [11]. Quadrature error cancellation, task (c), cannot be easily extrapolated to mode matched gyroscopes and is dependent on exact phase relations between signals corresponding to displacement and velocity in the two orthogonal directions.

When a gyroscope operates as an angle measuring transducer, it should be allowed to freely precess in response to the Coriolis force – no feedback strategies for compensation of precession can be effectively employed. However, the rate measuring gyroscope can operate in two different modes: the open loop mode and the force-to-rebalance mode. In the closed-loop mode, the control should be integrated with three control loops i.e. quadrature, energy and frequency tuning as proposed by Shkel et. al. is discussed in the next section.

The earliest control approach, proposed by Shkel et. al. [12], treats the gyroscope as a multi-degree of freedom device and compensates for a general class of quadrature errors and energy losses. The advantages were universal applicability to different gyroscope designs, robust quadrature cancellation scheme, feedback compensation of energy dissipation and on-line parameter tuning. Ellipticity of the gyroscope trajectory is undesirable because it directly enters into the measurements. Thus, as a general rule, zero ellipticity is desirable. Angular momentum and ellipticity (quadrature) is considered good measures of deviation from straight line oscillations.

$$P = \frac{1}{2}\oint(xdy - ydx) = \frac{1}{2}\int_0^{2\pi}(x\dot{y} - y\dot{x})dt$$
$$P = \pi(x\dot{y} - y\dot{x}) \qquad (5.2.1)$$

This measure of quadrature P was used for defining a quadrature compensating controller. The general goal of the quadrature control is to drive the area of the quadrature ellipsoid (5.2.1) to zero. Based on the classification of errors discussed in the previous chapter, the topology of the controller which will not interfere with the Corilois force, while compensating for the quadrature, should have the form

$$F_{quadr} = -\gamma_1.P.S^T.q \qquad (5.2.2)$$

where γ_1 is a constant gain, P is a quadrature defined by (5.2.1), S is a skew symmetric matrix and q is a displacement vector. This non-linear feeback control stabilizes the system to a manifold in the gyroscope phase space; the manifold corresponds to the straight line segment in (x,y) plane. In result of the quadrature control action, the area of the quadrature ellipsoid converges to zero, i.e. the ellipsoid approaches a straight line. The quadrature control does not affect the rate of the precession.

In addition to such a control, additional control is required to maintain constant overall energy of the system so that damping and other dissipative effects can be compensated. A control which will not interfere with the Coriolis force and will force the system to maintain the nominal energy level has the form

$$F_{energy} = -\gamma_2.\Delta E.\dot{q} \qquad (5.2.3)$$

This control force is proportional to the velocity and acts to cancel out the damping effects. This is primarily designed for absolute angle measurement.

An additional requirement is to match the fundamental frequencies of the system. This goal can be accomplished with the control

$$F_{tuning} = -\gamma_3.\Delta\omega.q \qquad (5.2.4)$$

The tuning control is a very important element in design of angular rate transducers because frequency mismatch directly defines the sensitivity of the device. In summary, it can be concluded that one of the necessary conditions for gyroscope operation is the stability of the nominal harmonic motion of the device and its insensitivity to external perturbations. Three coordinated feedback control actions were designed: the first is the control that minimizes quadrature errors equation (5.2.2), the second compensates for the energy variations equation (5.2.3) and the third tunes the frequencies of the system to a desirable value equation (5.2.4). All three controls are designed to compensate for manufacturing defects and electrostatic interferences. The feedback controller [13] is sufficient to compensate for imperfections while not interfering with the Coriolis force as long as the imperfections are sufficiently small (angle of misalignment $\alpha = 10^{o}$ and $h = 1\%$ of the ideal stiffness ($2h = K_1 - K_2$)). The results are depicted in Fig 5.2.1(a) and (b). The distinguishing feature of these controls is that they do not interfere with the measured Coriolis signal while performing assigned tasks.

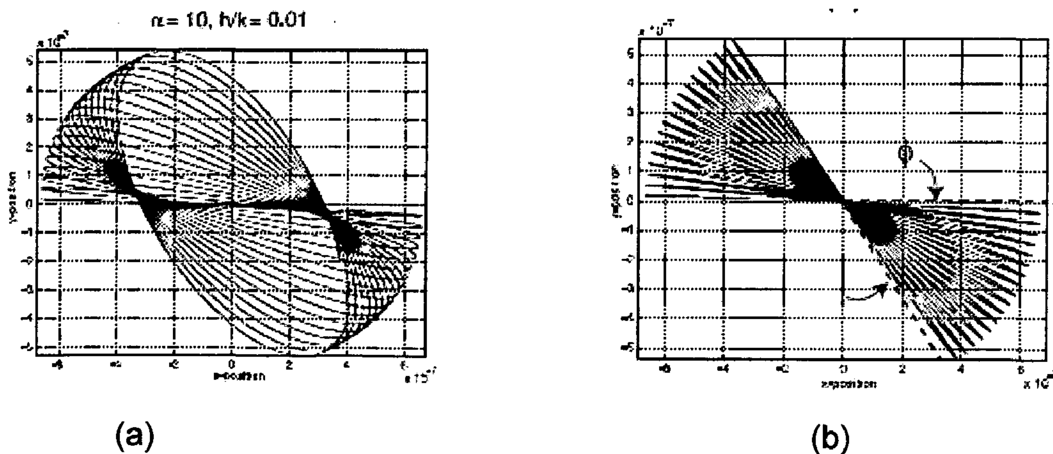

(a) (b)

Fig 5.2.1 (a) Anisoelasticities result in quadrature error which manifests as a developing elliptical pattern during precession of the straight line of oscillation.
(b) With the use of feedback control, these imperfections can be compensated for while preserving the angle of precession φ. Here, the angle of misalignment is 10° and the principal axes stiffness mismatch is 1% of the ideal isotropic stiffness Graphs obtained from [13].

The disadvantages in the control techniques are:-

(a) If off-diagonal elements in the damping matrix D are unknown, there will be errors in the estimation of angular velocity.

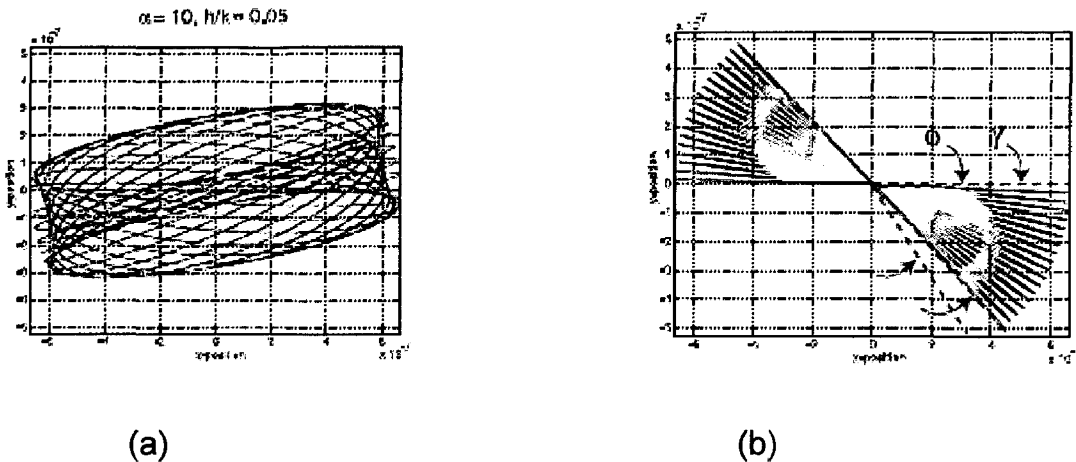

(a) (b)

Figure 5.2.2(a) Larger errors result in more erratic oscillation patterns, but can still be compensated for using the same feedback control. (b) However, the feedback control disrupts the line of oscillation, reducing the precession angle from the ideal angle φ to γ. Here the angle of misalignment is 10° and the principal axis stiffness mismatch is 5% of the ideal isotropic stiffness. From [13]

(b) However, typically if the imperfections are large (angle of misalignment α = 45° and h = 50% of the ideal stiffness) and while the controller will still compensate for the errors, it will interfere with the measured precession angle. (Refer Fig 5.2.2(a), (b) for α is 10 degrees and h = 5% of the ideal isotropic stiffness)

5.3 Sliding mode controller

There exists a cross coupling between the orthogonal axis of a vibrating MEMS gyroscope. The quantity to be measured, i.e. the angular velocity of the proof mass, is an unknown disturbance term to the controller which has to maintain the proof mass to vibrate at fixed amplitude and frequency. An adaptive model reference and a sliding mode controller were proposed by Batur et. al [14] to estimate the unknown angular velocity and control the motion of the proof mass.

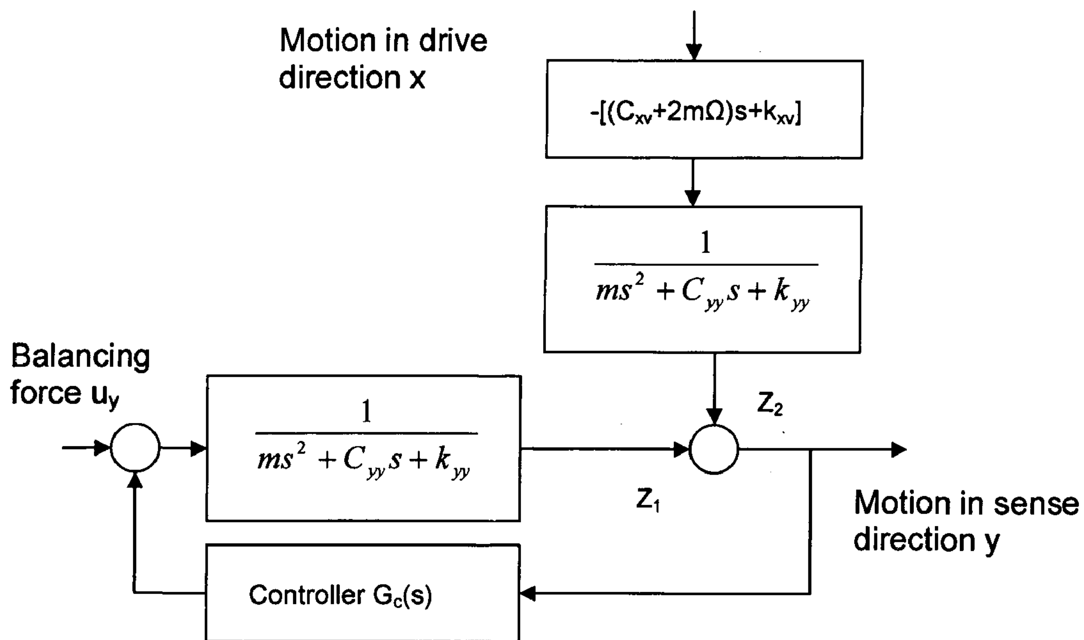

Fig 5.3.1 Force balancing controller

The feedback control to stabilize the loop in the sense direction (y) is shown in Fig 5.3.1. The controller $G_c(s)$ is designed to maintain $z_1 = -z_2$ at the operating frequency in the drive direction, therefore the effect of the motion in the drive direction can be cancelled. In this paper, it was shown that a Lyapunov function based model reference controller can maintain the proof mass at the desired amplitude and frequency, therefore the tracking error goes to zero. All signals within the control system, including the estimation error, remain bounded. However, estimation of the angular velocity will approach the true value under certain assumptions since the Lyapunov stability theorem can only guarantee the boundedness of signals.

If the uncertainties of the system can be estimated, then a sliding mode controller on the drive direction and a force balance controller on the sense direction can be constructed to consistently estimate the unknown angular velocity.

5.4 Active Disturbance Rejection Control (ADRC)

Most control approaches for MEMS gyroscopes employ various methods to derive the accurate model of the plant. In practice, it is very challenging to achieve the precise model information. Especially for MEMS gyroscope, the factors such as the mechanical-thermal noise, the measurement noise, the unknown time varying rotation rate and the unknown quadrature error terms bring modeling errors and structural uncertainties in the system. The mechanical imperfection and environmental variations also introduce the parameter variations to the model of MEMS gyroscopes. ADRC [14] is a natural fit for the MEMS gyroscope control due to its inherent disturbance rejection characteristics.

The system equation of MEMS gyroscope can be rewritten as

$$\begin{aligned} \ddot{x} &= -(2\zeta\omega_n\dot{x} + \omega_n^2 x + \omega_{xy} - 2\Omega\dot{y}) + b_x u_d \\ \ddot{y} &= -(2\zeta_y\omega_y\dot{y} + \omega_y^2 y + \omega_{xy}x + 2\Omega\dot{x}) + b_y u_s \end{aligned} \tag{5.4.1}$$

where $b_x = b_y = \frac{k}{m}$

Define

$$\begin{aligned} f_x &= -(2\zeta\omega_n\dot{x} + \omega_n^2 x + \omega_{xy} - 2\Omega\dot{y}) \\ f_y &= -(2\zeta_y\omega_y\dot{y} + \omega_y^2 y + \omega_{xy}x + 2\Omega\dot{x}) \end{aligned} \tag{5.4.2}$$

Where f_x and f_y are referred to as the generalized disturbance because they represent both the unknown internal dynamics and the external disturbances of the drive and sense axes respectively. The couplings between the two axes are also taken as disturbances to each axis. Substituting (5.4.2) into (5.4.1), the system becomes

$$\begin{aligned} \ddot{x} &= f_x + b_x u_d \\ \ddot{y} &= f_y + b_y u_s \end{aligned} \tag{5.4.3}$$

The basic idea of ADRC is to obtain the estimated f_x and f_y, i.e. $\hat{f}_x, \hat{f}_y$ and then to compensate for them in the control law in real time. The control designs of the drive and the sense axes are the same and they are implemented in parallel.

The steps for implementing ADRC are first design a extended state observer so that all the observer poles are placed at $-\omega_{xy}$. This makes ω_{xy} the only tuning parameter for the observer thereby simplifying observer implementation. Once the observer is designed and tuned, its outputs will track $y, \dot{y}, f_y$ respectively. By canceling the effect of f_y, ADRC actively compensates for f_y in real time. The original plant equation reduces to $\ddot{y} = u_0$, which is a much simple control problem to deal with. A simple controller can be designed then. A feedforward mechanism is employed for the purpose of reducing the tracking error. The controller gains are selected so that the closed loop characteristic polynomial is Hurwitz. For tuning simplicity, all the controller poles are placed at $-\omega_{xy}$. Then the approximate closed loop characteristic polynomial is $(s+\omega_{cy})^2$. This makes $-\omega_{cy}$, the controller bandwidth, the only tuning parameter for the controller of the sense axis. This is called bandwidth parameterization which simplifies the control system design.

ADRC approach is used to control the drive and sense axes of a vibrational MEMS gyroscope. Based on the accurate estimation of the internal plant dynamics and external disturbances of ESO, a demodulation technique is used to estimate the time varying rotation rate. Since the ADRC does not require an accurate mathematical model of the plant, it is a good fit for the control and rate estimation of the MEMS gyroscope in the presence of noises and parameter variations. ADRC minimizes the effect of fabrication imperfections.

5.5 Adaptive Mode Tuning for Vibrational Gyroscopes

In Section 5.1 it was mentioned that phase locked loop is used for frequency stability. An adaptive controller was proposed by Robert P Leland [18] in 2003 for tuning the natural frequency of the drive axis of a vibratinal gyroscope. This is an attractive alternative to a phase locked loop, since it introduces feedback, which can reduce the effects of imprecise fabrication. Also, the gyroscope can be operated at a fixed frequency, chosen by the designer, which can simplify signal processing.

Most MEMS gyroscopes are driven at resonance in order to obtain a large response and to enable phase synchronization. A phase locked loop is used to adjust the input frequency until the drive axis output is -90° out of phase with the input, indicating resonance for a second order system with no zeros. Thus, the input frequency depends on the mechanics of the device, and changes with temperature or other environmental factors.

In the proposed technique, the gyroscope is placed in a feedback loop, and the feedback gain is adapted to force the output to be -90° out of phase with the input, indicating resonance. This approach has two advantages:-

(a) Resonant frequency is chosen by the designer and can be incorporated into the signal processing design.

(b) Feedback can reduce the effect of nonlinearities and other uncertainties.

Control of the resonant frequency is needed for two reasons:-

(a) The resonant frequencies of the drive and sense axes must be matched precisely, due to the sharp resonant peak. The accuracy required is well beyond the fabrication tolerance for these lightly damped systems.

(b) The resonant frequencies change with temperature, due to thermal expansion or change in Young's modulus. The coefficient of thermal expansion for single crystal silicon is relatively small, but frequency shifts are still a significant factor.

Feedback control is used in vibrational gyroscopes to

(a) regulate the amplitude of the drive axis vibration (automatic gain control)

(b) compensate for coupling of the drive and sense axes (quadrature cancellation)

(c) operate the gyro at resonance (phase locked loop on the drive axis and mode tuning on the sense axis).

In this approach the controller is non-linear and the coefficients of the feedback terms are adapted. No observers are used in this technique. Also, in this case only the operation of the drive axis at resonance is controlled and not the whole gyro operation. This controller is intended for force-to-rebalance operation.

5.5.1 Gyroscope Drive Axis Model

An ideal gyroscope, with no coupling between the drive and sense axes, and similar dynamics on both axes is modeled as

$$\begin{aligned} \ddot{x} + 2\varsigma\omega_n\dot{x} + \omega_n^2 x + 2\Omega\dot{y} &= \frac{1}{m}u_{drive}(t) \\ \ddot{y} + 2\varsigma\omega_n\dot{y} + \omega_n^2 y - 2\Omega\dot{x} &= \frac{1}{m}u_{sense}(t) \end{aligned} \qquad (5.5.1)$$

where x(t) is the drive axis displacement, y(t) is the sense axis displacement, Ω is the rotation rate about the z axis, u_{drive} and u_{sense} are the control inputs for the drive and sense axes, m is the mass of the vibrating element, $2\Omega\dot{x}$ and $2\Omega\dot{y}$ are the Coriolis acceleration. Rotation sensing is achieved by forcing the drive axis

into a fixed amplitude vibration and measuring the displacement y(t) of the sense axis. Typically, the Coriolis force on the drive axis is negligible. Hence the drive axis is described by

$$\ddot{x} + 2\varsigma\omega_n\dot{x} + \omega_n^2 x = \frac{1}{m}u_{drive}(t) \qquad (5.5.2)$$

This system is put in a feedback loop, by taking $u_{drive}(t) = k(r(t) - \hat{K}x(t))$, with reference input r(t) and variable feedback gain $\hat{K}$ as shown in Fig 5.5.1

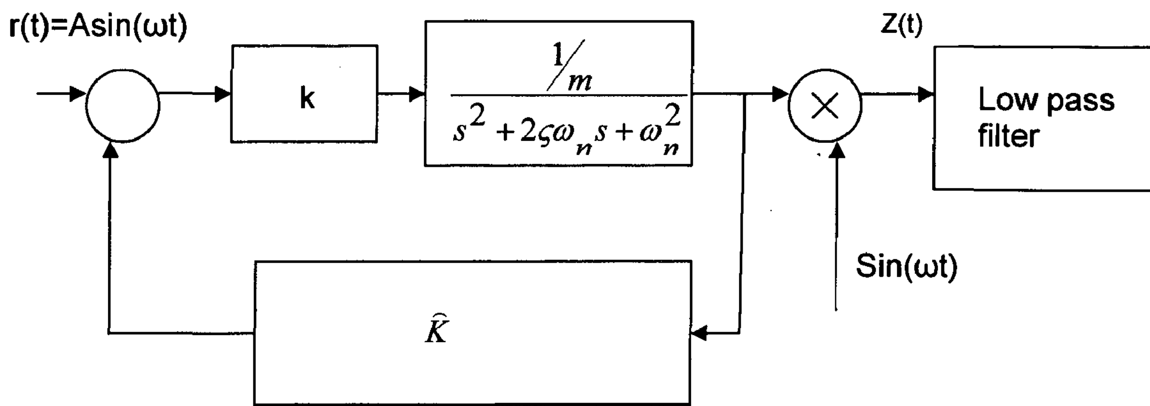

Fig 5.5.1 Feedback loop with adaptive control gain $\hat{K}$

5.5.2 Resonant Gain

It is critical to maintain an adequate gain at resonance in order to obtain a sufficiently large vibration. For the open loop system, with just the gyro

$$G(s) = \frac{X(s)}{U_{drive}(s)} = \frac{1/m}{s^2 + 2\varsigma\omega_n s + \omega_n^2} \qquad (5.5.2.1)$$

Then $|G(j\omega_n)| = 1/2\varsigma\omega_n^2 m$. The closed loop system transfer function is

$$T(s) = \frac{X(s)}{R(s)} = \frac{k/m}{s^2 + 2\varsigma\omega_n s + \omega_n^2 + \hat{K}k/m} \qquad (5.5.2.2)$$

which has natural frequency $\omega_1 = \sqrt{\omega_n^2 + \hat{K}k/m}$.

The change in the gain at resonance due to feedback is

$$\left|\frac{T(j\omega_1)}{G(j\omega_n)}\right| = \frac{k\omega_n}{\sqrt{\omega_n^2 + \hat{K}k/m}} \quad (5.5.2.3)$$

While the gain at other frequencies is substantially reduced, the gain at resonance is not substantially reduced by feedback.

5.5.3 Adaptive control for resonance

An adaptive controller to place the resonant frequency of the closed loop system, ω_1, at the frequency of a given input sinusoid is designed here. Suppose the input to the system is $r(t) = A\sin(\omega t)$. Assume $\hat{K}$ is slowly varying and can be treated as a constant, the gyroscope output is

$$x(t) = |T(j\omega)\ (A\sin(\omega t + |\text{angle } T(j\omega)) + \text{transient} \quad (5.5.3.1)$$

Initially, it is assumed that the transient has decayed and only the steady state sinusoidal output remains. The adaptation law should drive the angle of $T(j\omega)$ to -90°. As shown in Figure 5.5.1, a phase detector is implemented by multiplying x(t) by $\sin(\omega t)$ to obtain z(t) = x(t) $\sin(\omega t)$. Then

$$z(t) = \frac{1}{2}|T(j\omega)|(A\cos(\text{angle } T(j\omega)) - A\cos(2\omega t + \text{angle } T(j\omega))) \quad (5.5.3.2)$$

In theory an ideal low-pass filter with a gain of two and cutoff frequency well below 2ω is applied to z(t) as in Figure 5.5.1. The filter output is then

$$s(t) = A\frac{\tilde{K}}{\tilde{K}^2 + \frac{m^2}{k^2}4\varsigma^2\omega_n^2\omega^2} \quad (5.5.3.4)$$

where $\hat{K}^* = \left(\frac{m}{k}\right)\left(\omega^2 - \omega_n^2\right)$ is the ideal value for $\hat{K}$, and $\tilde{K} = \hat{K} - \hat{K}^*$ is the parameter error.

The following adaptation law is used.

$$\dot{\hat{K}} = -\gamma s(t) \tag{5.5.3.5}$$

which yields approximate error dynamics

$$\dot{\hat{K}} = \frac{-A\gamma}{\tilde{K}^2 + \frac{m^2}{k^2}4\varsigma^2\omega_n^2\omega^2}\tilde{K} \tag{5.5.3.6}$$

The adaptation gain $\dot{\hat{K}}/\tilde{K}$ increases rapidly near resonance. For sufficiently large γ this leads to instability or limit cycles in $\hat{K}$. This is due to the dynamics of the gyroscope transient response, adaptation law and low-pass filter that were omitted from the analysis. First the low pass filter is omitted to maintain stability and keep γ small so the high frequency oscillation in $\hat{K}$ is acceptable. Secondly, a nonlinear phase detector with a saturation element to limit the adaptation rate is utilized. The results are simulated in MATLAB/SIMULINK and are discussed in Chapter 6.

Simulation Results

6.1 Ideal gyroscope

A generic model of an oscillating system that exhibits the motion discovered by Foucault is given by the coupled system of differential equations

$$\begin{aligned} \ddot{x} + \omega_n^2 x - 2\Omega\dot{y} = 0 \\ \ddot{y} + \omega_n^2 y + 2\Omega\dot{x} = 0 \end{aligned} \quad (6.1.1)$$

Physically x and y represent the Cartesian coordinates of a point on the longitudinal axis of the vibrating member measured in a plane fixed in this instrument and normal to the axis. The parameter ω_n is the frequency of vibration, Ω is the angular velocity of rotation of the member about the longitudinal axis. The essential feature of these equations is the presence of Coriolis accelerations $-\Omega\dot{y}$ and $\Omega\dot{x}$. These two terms will appear only if the equations of the motion are written in a non-inertial coordinate frame. It is the Coriolis acceleration that is responsible for the Foucault effect.

There are many physical systems including vibrating strings, rods and rings, the ideal motion of which is characterized by equation (6.1.1). All such systems will exhibit the gyroscopic effect discovered by Foucault. If the input angular velocity is zero, and under appropriate initial conditions, the ideal gyroscope will oscillate along a straight line. The orientation of the straight line is defined by initial conditions.

By substituting the values of k=1.55, m=4.1e-10 in $m\ddot{x} + kx = 0, m\ddot{y} + ky = 0$, the solution of the equation is

source?

x = C3*sin(50000/41*2542^(1/2)*t)
y = -C1*sin(50000/41*2542^(1/2)*t)

where m is the mass of the gyroscope, k is the stiffness coefficient in N/m and C1, C3 are constants. The values were put in an M-file in MATLAB and the plot (x,y) obtained is shown in Fig 6.1.1

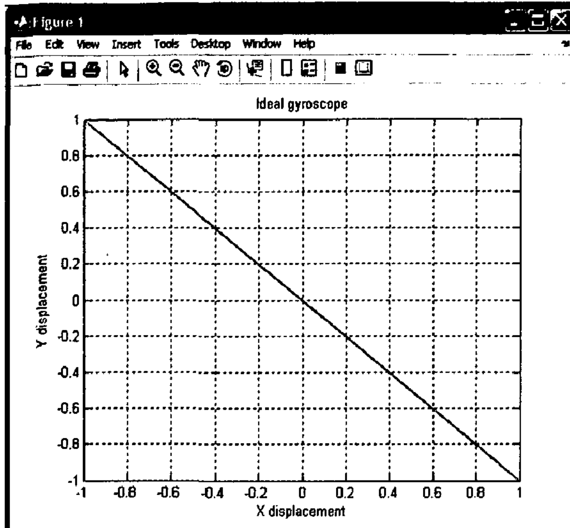

Fig 6.1.1 Ideal gyroscope

In a more general case, when the initial conditions are such that the vector of displacement is not parallel to the vector of velocity, the orbit of the gryroscope motion is an ellipse. The solution when $\Omega = 0$ is given by

$$\begin{aligned}
x &= a\cos\theta\cos\phi - b\sin\theta b\sin\phi \\
y &= a\cos\theta\sin\phi + b\sin\theta\sin\phi \\
\dot{x} &= \omega_n(-a\sin\theta\cos\phi - b\cos\theta\sin\phi) \\
\dot{y} &= \omega_n(-a\sin\theta\sin\phi + b\cos\theta\cos\phi)
\end{aligned} \qquad (6.1.2)$$

The parameters a,b, θ and ϕ are constants that depend on the initial conditions: a and b define the shape of the ellipse, ϕ defines the orientation of the ellipse and θ_0 defines the location of the gyroscope reference point on the ellipse at the initial instant. The parameters are depicted in the figure 6.1.2. θ is the angle measured on a circle of radius a between the ascending apsis A and the point B located at the intersection of the circle with a line parallel to the minor axis through the point (x,y). The point B is not physically identifiable but has the convenient property of moving at the constant angular velocity Ω.

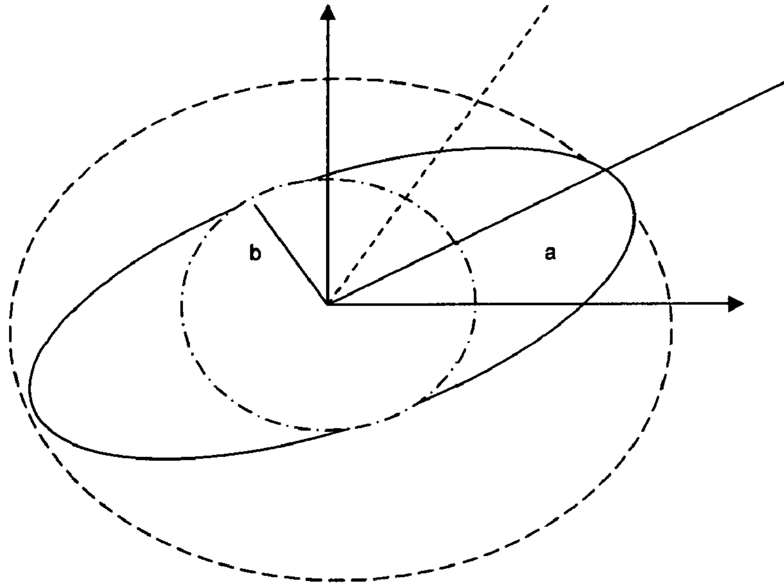

Fig 6.1.2 Orbital elements of a vibrating member

In equation (6.1.2), put the value of a=1, b=0, θ is varied from –pi to +pi and so is ϕ. The plot of (x,y) for the values were obtained through MATLAB and is shown in Fig 6.1.3. As seen in the figure, the value of a affects only the semi-major axis of the ellipse. The diameter of the semi-major axis is the value of a.

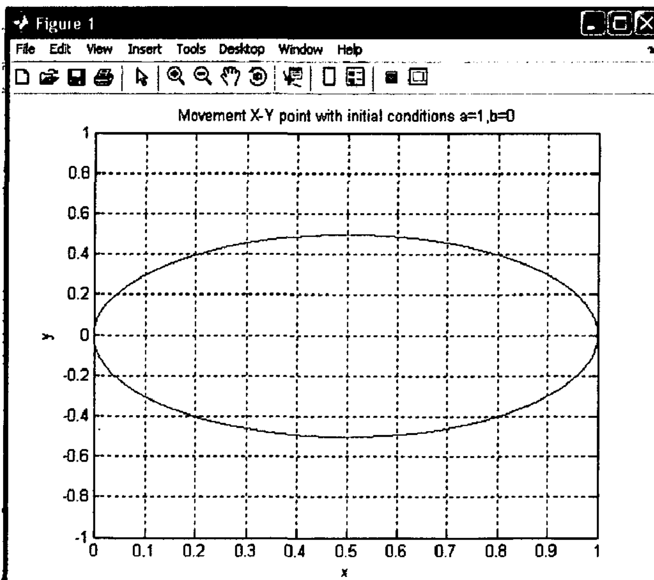

(a)

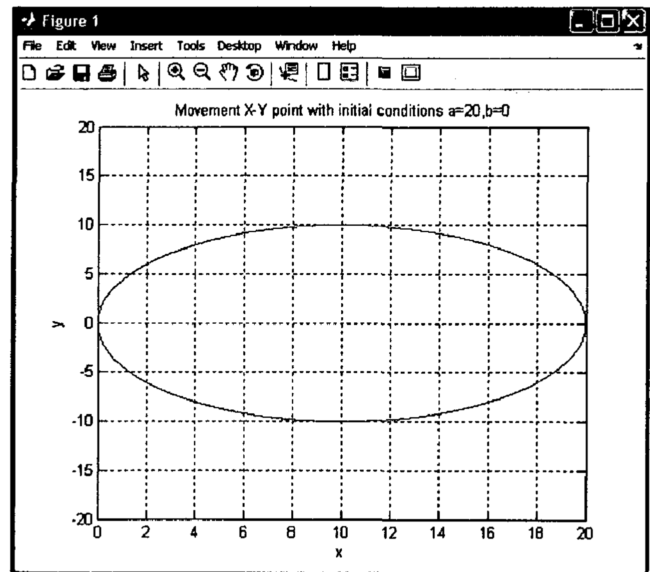

(b)

Fig 6.1.3 Ellipse motion of the point (x,y) when (a) a=1 and b=0 (b) a=20 and b=0

Holding the value of a=20 and if we increase the value of b (semi-minor axis), the shape of the ellipse is changed and is shown in Fig 6.1.4.

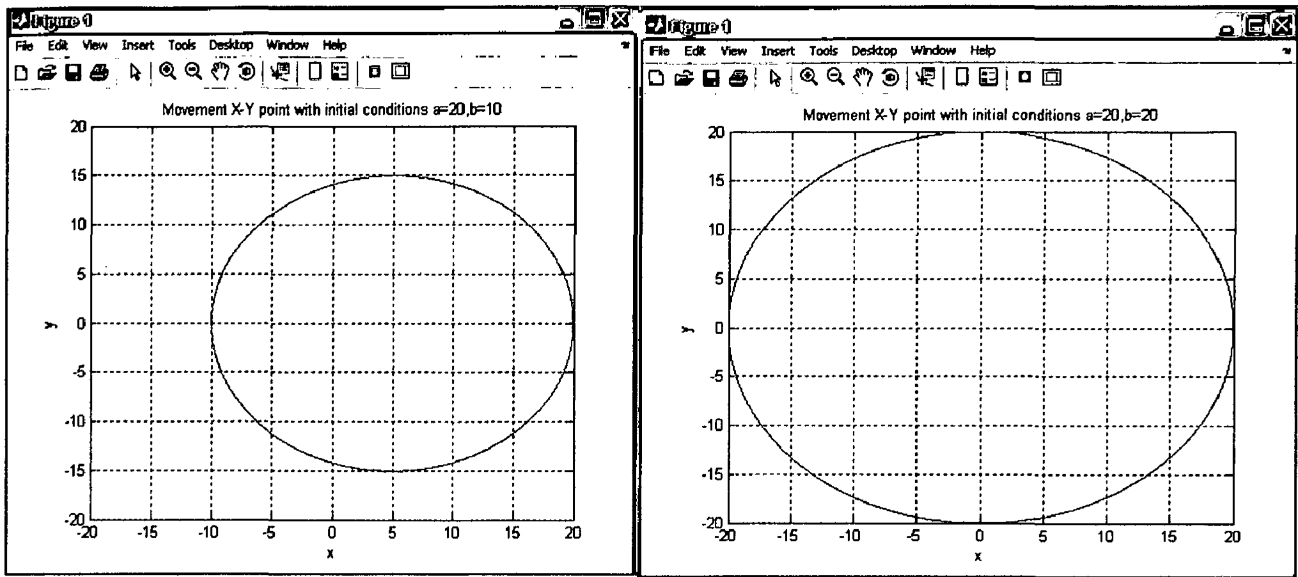

(a) (b)

Fig 6.1.4 (a) Ellipse when a=20, b=10 (b) Circle when a=b=20

6.2 Non-ideal gyroscope

The governing equation of a non-ideal dynamical system is

$$\begin{bmatrix} m & 0 \\ 0 & m \end{bmatrix}\begin{pmatrix} \ddot{x} \\ \ddot{y} \end{pmatrix} + \begin{bmatrix} C_{xx} & C_{xy} - 2m\Omega \\ -C_{yx} + 2m\Omega & C_{yy} \end{bmatrix}\begin{pmatrix} \dot{x} \\ \dot{y} \end{pmatrix} + \begin{pmatrix} K_{xx} & K_{xy} \\ K_{yx} & K_{yy} \end{pmatrix}\begin{pmatrix} x \\ y \end{pmatrix} = \begin{pmatrix} F_x \\ F_y \end{pmatrix} \tag{6.2.1}$$

where m is the lumped mass approximation for the gyroscope, K_{xx}, K_{xy}, K_{yx},and K_{yy} are the non-ideal stiffness terms, C_{xx}, C_{xy}, C_{xy} and C_{yy} are the non-ideal damping terms and F_x and F_y are applied forces. Non-idealities that vary with position and velocity can also be referred as anisoelasticity and anisodamping.

The off diagonal elements in the stiffness matrix appear when the main axes of elasticity do not coincide with the coordinate system {x y}. By analogy with stiffness, damping can also be described in terms of two main axes of damping. In general, the principal axes of elasticity and damping are not necessarily aligned because asymmetry in stiffness and damping are caused by different

physical phenomena. Thus, off-diagonal elements in the damping matrix also appear due to misalignment of the main axes of damping with the coordinate axes {x y}.

6.2.1 Stiffness

The effect of anisoelasticity is simulated with the help of MATLAB/SIMULINK. Anisoelasticity occurs due to the presence of non-zero terms in the off-diagonal stiffness matrix. Presence of zero terms in the off-diagonal elements results in a straight line oscillation and in case if an external angular input rate is given it results in precession of the straight line. The results are shown in Fig 6.2.1(a).

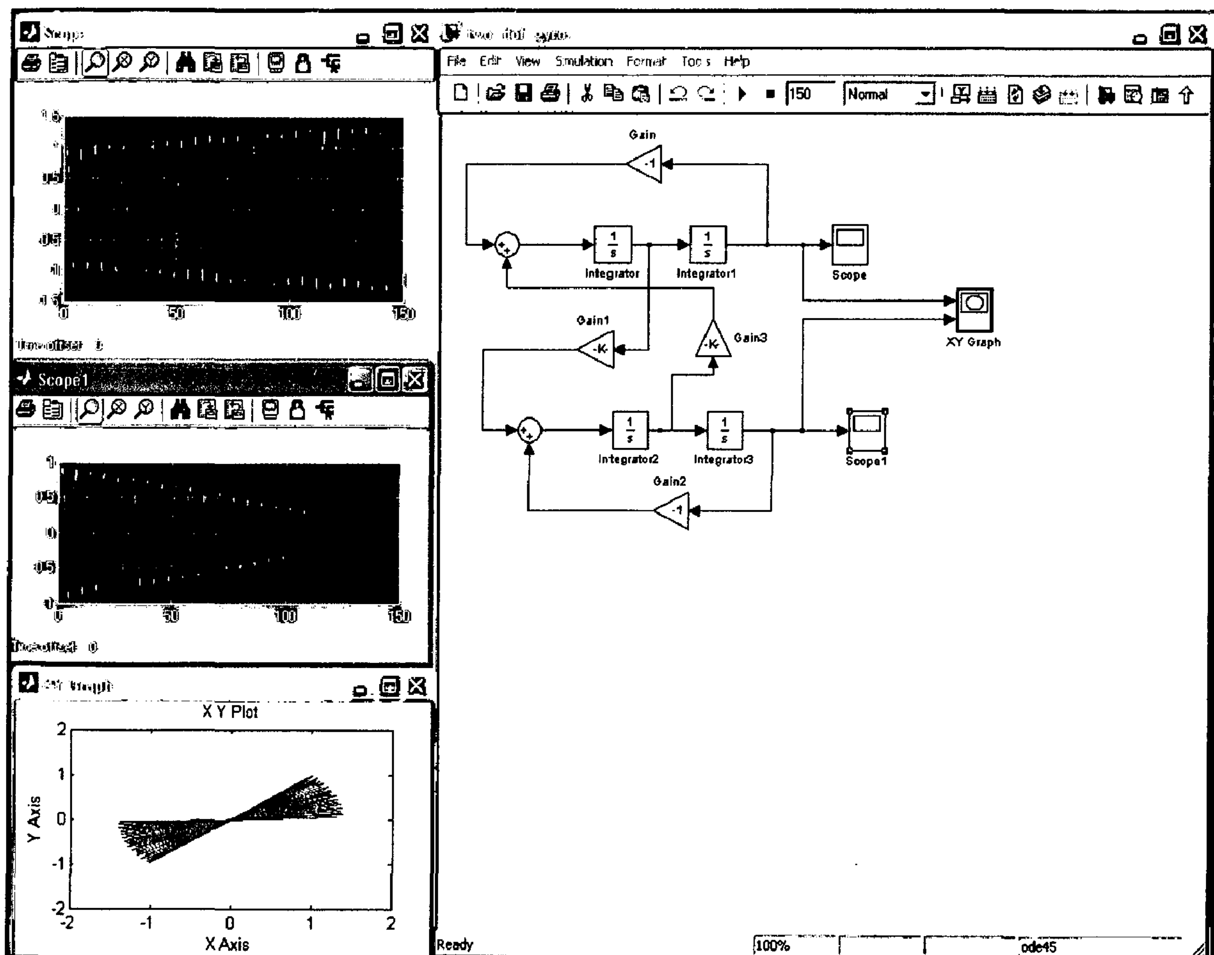

Fig 6.2.1 (a) Precession of straight line due to non-zero off diagonal terms in stiffness matrix

In a surface machined rate integrating gyroscope consisting of a freely vibrating proof mass attached to a concentric six ring suspension system, stationary electrodes are interwoven throughout the mass along the drive axes. This helps to sustain motion while electrodes along the sense axes sense deflection and velocity used to calculate the Coriolis induced deflection angle. In this operation, Coriolis force causes the line of oscillation initially aligned with the horizontal axis attached to the rotating frame to precess by an angle ϕ.

However, a small variation of off-diagonal elements that is 1% (of ideal stiffness) variation not only affects the straight line oscillation but results in erroneous calculation of angular velocity. The alteration in the straight line is shown in Fig 6.2.1(b).

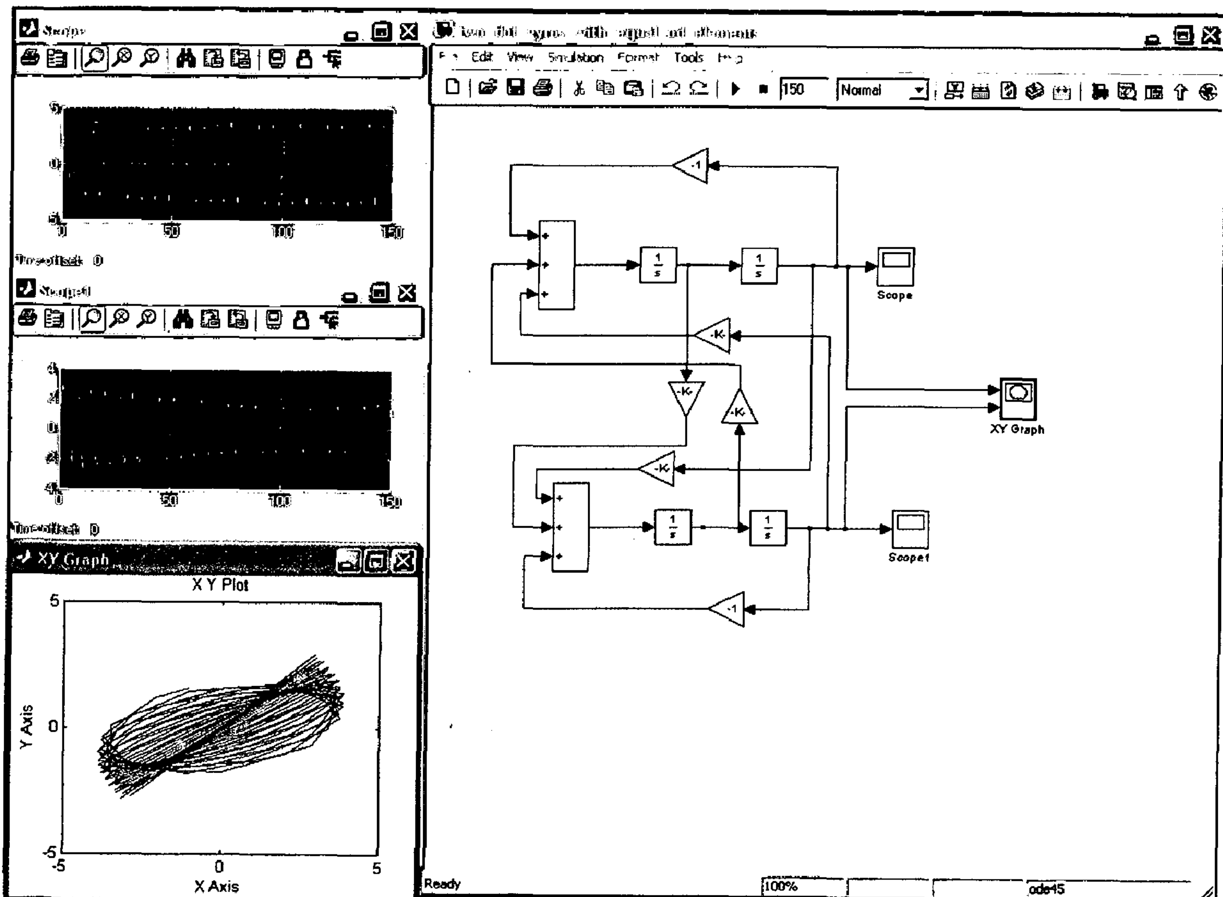

Fig 6.2.1(b) With 1 per cent variation in the off-diagonal elements, the plot of (x,y) is a precessing ellipsoid instead of a straight line.

However, a further variation of off-diagonal elements that is 5% (of ideal stiffness) variation in the straight line is shown in Fig 6.2.1(c)

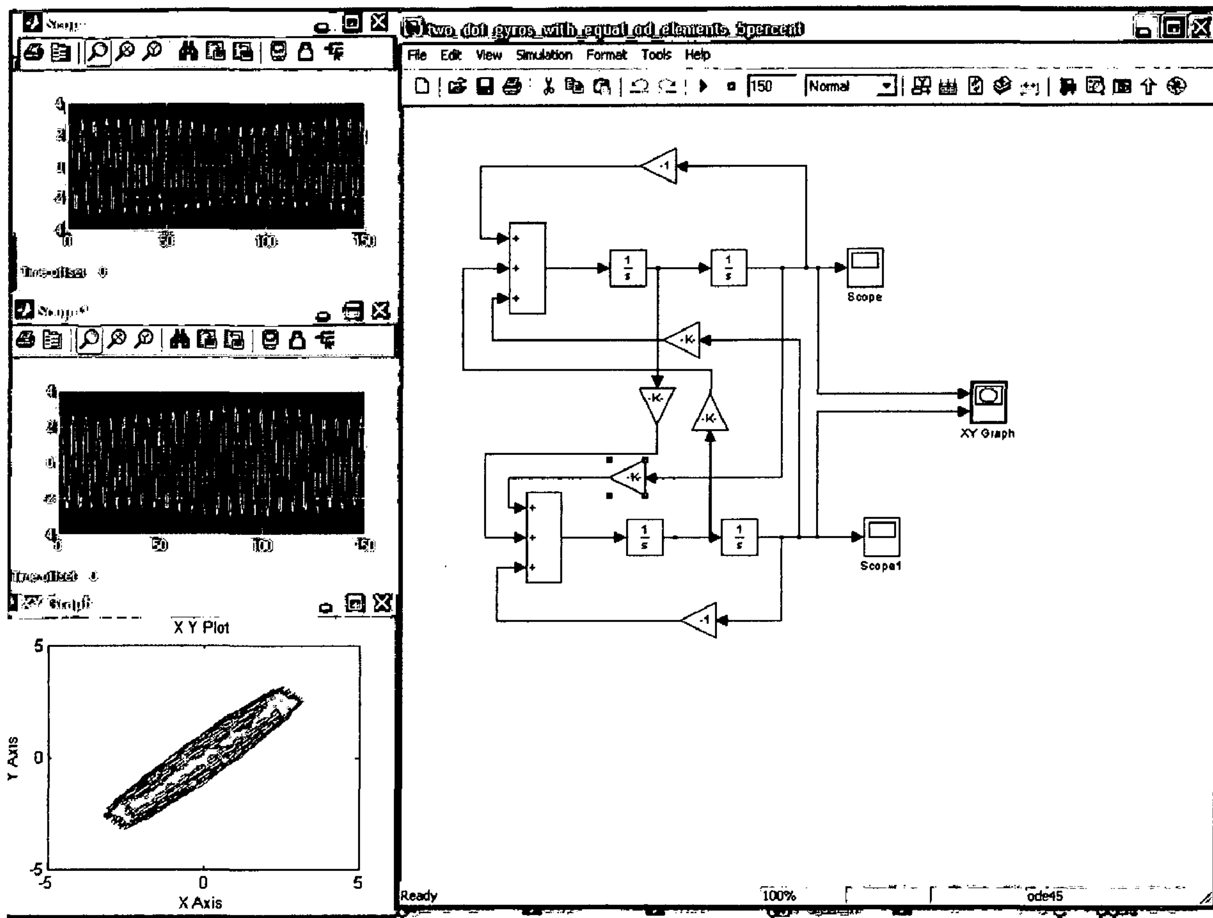

Fig 6.2.1(c) Variation of 5% in the off-diagonal elements

The conclusion of this simulation work is that off-diagonal elements in the stiffness matrix affect the performance of the gyroscope resulting in improper calculation of angular velocity. This is primarily due to the disruption of straight line oscillation. Off-diagonal elements in the stiffness matrix result in frequency change and disruption of the straight line oscillation. Spherical forces (diagonal stiffness matrix) cause only frequency change. Hyperbolic potential forces (positive definite stiffness matrix) cause frequency change as well as disruption of straight line oscillation. Non-potential forces can appear only if off-diagonal elements in the stiffness matrix are not equal. These forces also cause disruption

of the straight line oscillation but do not result in frequency change. This is shown in Fig 6.2.1(d)

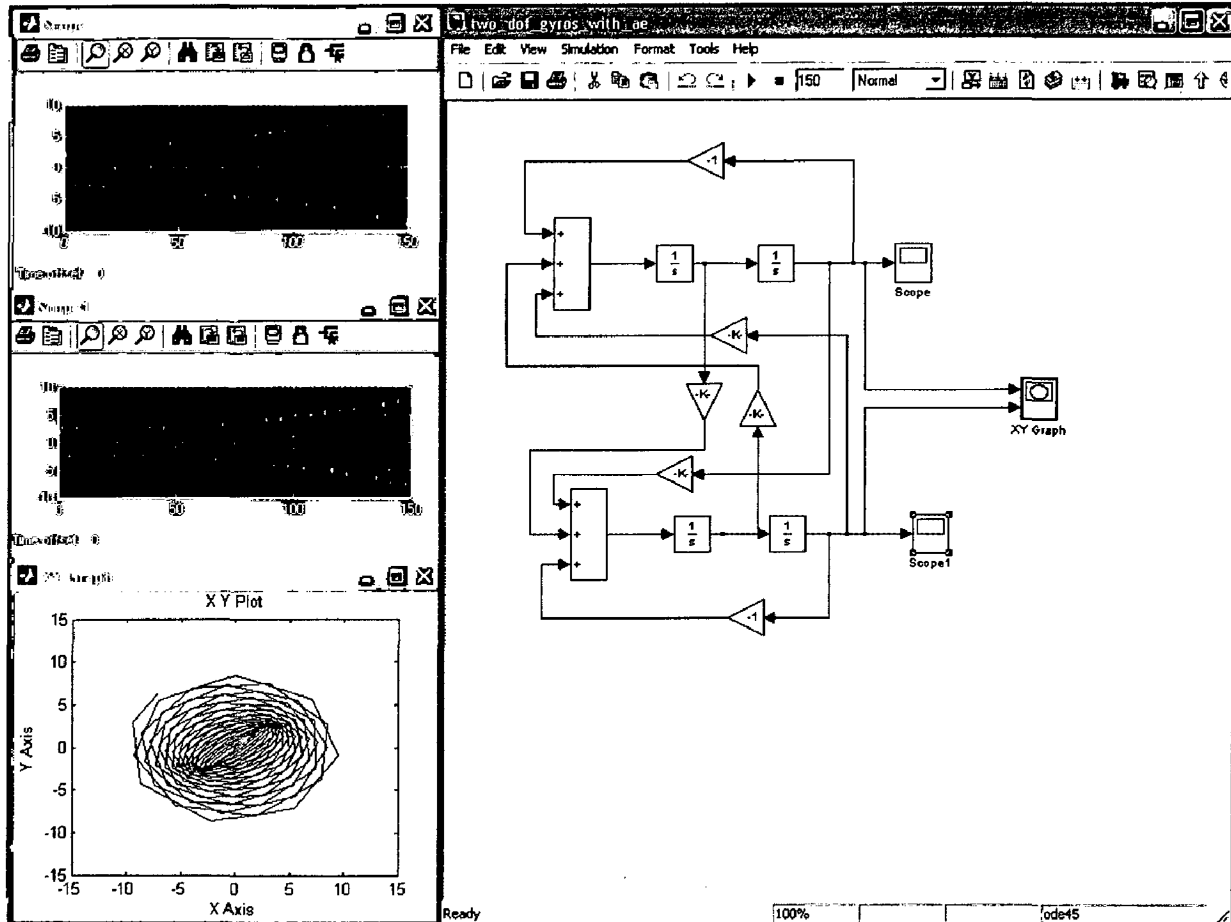

Fig 6.2.1(d) Effect of non-potential forces due to unequal off-diagonal elements in the stiffness matrix.

6.2.2 Damping

The gyroscope is a dynamic device moving in a two dimensional working plane, topology of damping within the system is also important. Nonideal topologies consist of damping asymmetries and coupling between principal axis of operation. Due to scaling laws, the damping effects that are negligible in macro world devices become very significant in micro scale devices. The effect of anisodamping is simulated with the help of MATLAB/SIMULINK. Anisodamping occurs due to the presence of non-zero terms in the off-diagonal damping matrix.

Asymmetry in damping can be presented in the form of dissipative spherical forces, dissipative hyperbolic forces and gyroscopic forces. Dissipative spherical forces cause only amplitude change. Hyperbolic velocity dependent forces result in precession of the straight line oscillation and amplitude change. The damping matrix has unequal diagonal and off-diagonal values. The results are shown in Fig 6.2.2(a).

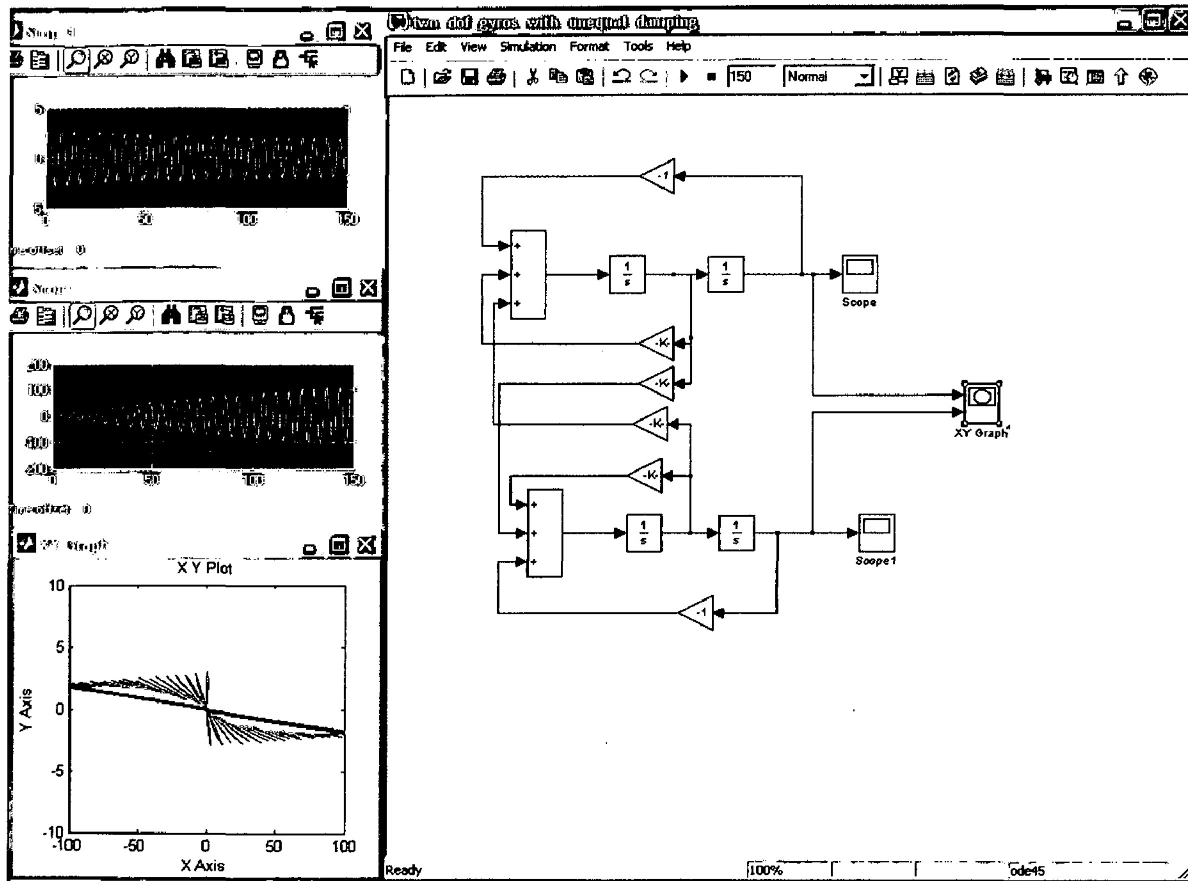

Fig 6.2.2(a) Hyperbolic velocity dependent forces due to damping results in precession of the straight line oscillation and amplitude change.

Gyroscopic forces can cause only precession as shown in Fig 6.2.2(b). Dissipative spherical forces and hyperbolic forces can appear as a result of losses due to structural damping, transmission of energy to suspension, aerodynamic drag etc. Gyroscopic forces can appear only as inertial forces.

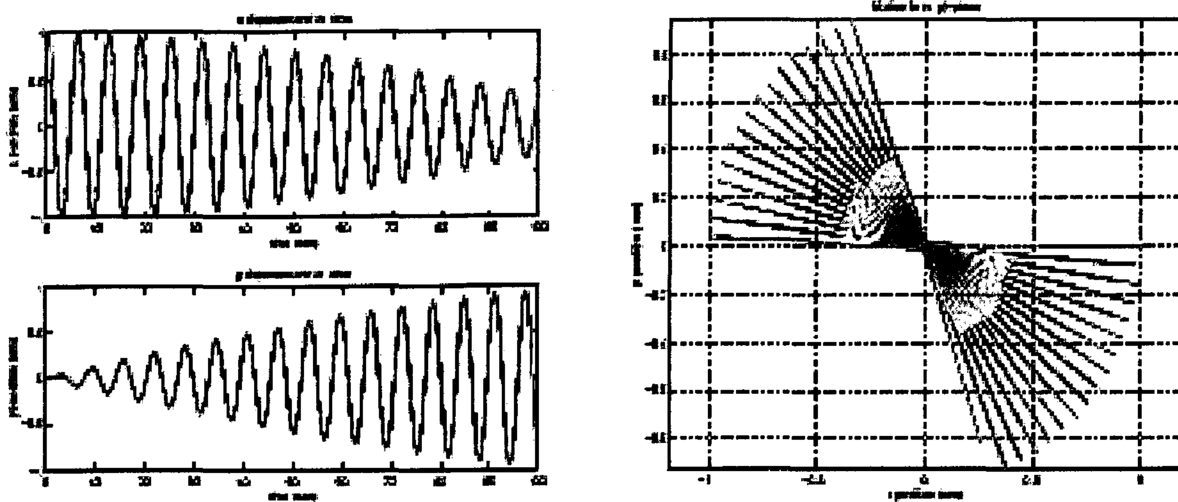

Fig 6.2.2(b) Effect of gyroscopic force in damping matrix. Reproduced from [8]

The conclusion of the simulation is that off diagonal symmetric elements in the damping matrix result in precession of straight line oscillation and amplitude change. Skew-symmetric terms in the damping matrix cause only precession of the gyroscope line of oscillation. The effect of off-diagonal damping elements is not distinguishable from the effect of the Coriolis force, and thus present significant difficulties.

The most dangerous perturbations for the gyroscope operation are hyperbolic potential forces, non-potential forces, hyperbolic velocity dependent forces and gyroscopic like forces appearing as off-diagonal elements in the damping matrix.

6.3 Adaptive Mode Tuning

Adaptive control scheme for Mode Tuning [18] discussed in Chapter 5.5 was simulated using SIMULINK. The gyroscope model was taken from experimental measurements of a flexible beam gyroscope, built as a prototype at the University of Alabama. The gyro consists of a 50mm long steel beam with square cross section. Piezoelectric strips are attached to each side as either sensors or actuators. The beam is supported with wires at the nodes of its first bending mode, so this mode behaves like that of a free-free beam. The first bending

mode is excited which has a natural frequency of 10.167 KHz and a damping ratio of $\varsigma = 0.0005$. Block diagrams of the system are shown in Fig 6.3.1 and Fig 6.3.3. The gain in the numerator of the drive axis transfer function includes mass, actuator and sensor scale factors. The driving frequency was 10.5 KHz. The forward gain was taken to be 11.1 in order to make the ideal feedback gain $\hat{K}(0) = 0$.

6.3.1 Adaptive tuning with linear phase detector

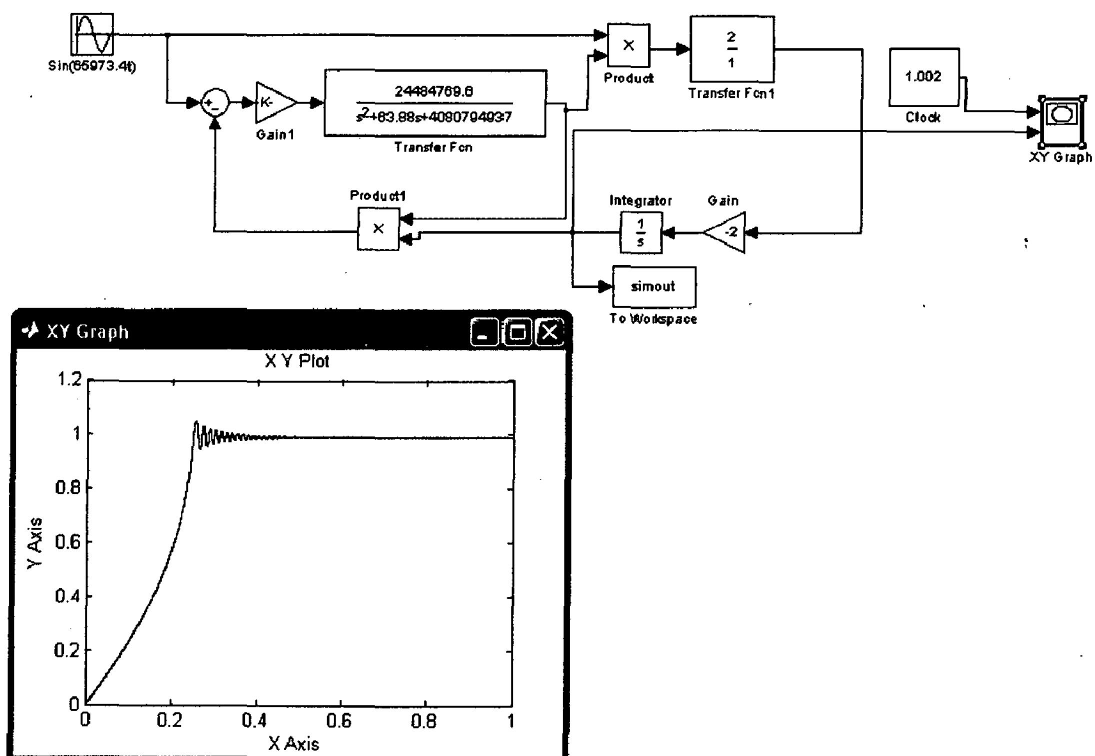

Figure 6.3.1 Adaptive tuning with linear phase detector and no low pass filter. Graph depicts $\hat{K}$ versus time.

The gyroscope with the adaptation law and phase detector described in Chapter 5.5 was simulated. A Simulink diagram of this simulation is shown in Fig 6.3.1. The use of a low pass filter in the phase detector led to unexpected limit cycles and instability for higher values of adaptation rate γ. This is primarily due to peaking of the adaptation rate near resonance. Away from resonance the system

worked as expected. Removing the low pass filter yielded acceptable performance, but with slower adaptation and a larger high frequency component in $\hat{K}$. The filtered phase detector output versus time is shown in Fig 6.3.2

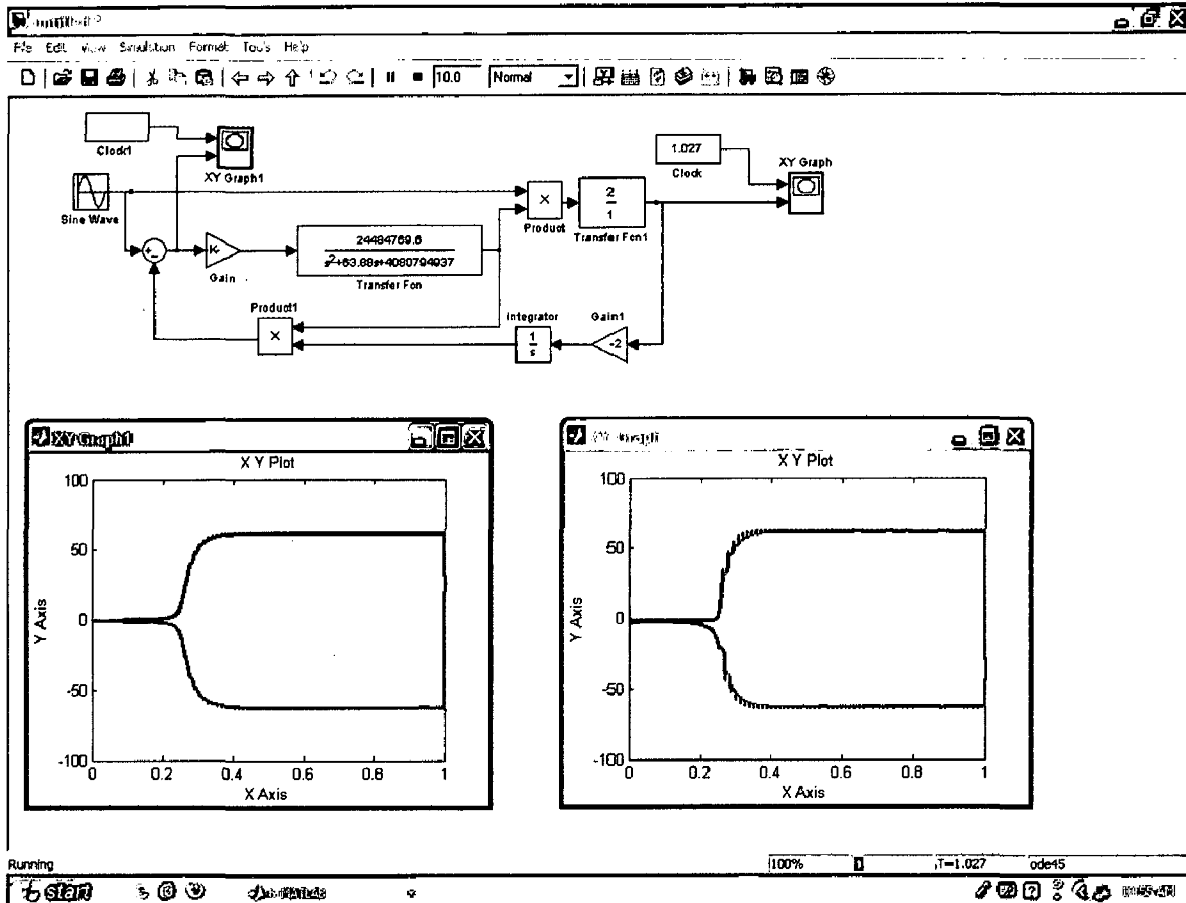

Fig 6.3.2 Adaptive tuning with linear phase detector and no low pass filter. Graph depicts error input vs time (XY Graph1) and filtered output vs time (XYGraph)

6.3.2 Adaptive tuning with saturating phase detector

To avoid peaking in the adaptation rate, a saturation element and a high gain is introduced in the phase detector as shown in Fig 6.3.3 and Fig 6.3.4. This led to a rapid, highly accurate response, as a low pass filter could be included to reduce the high frequency component of $\hat{K}$.

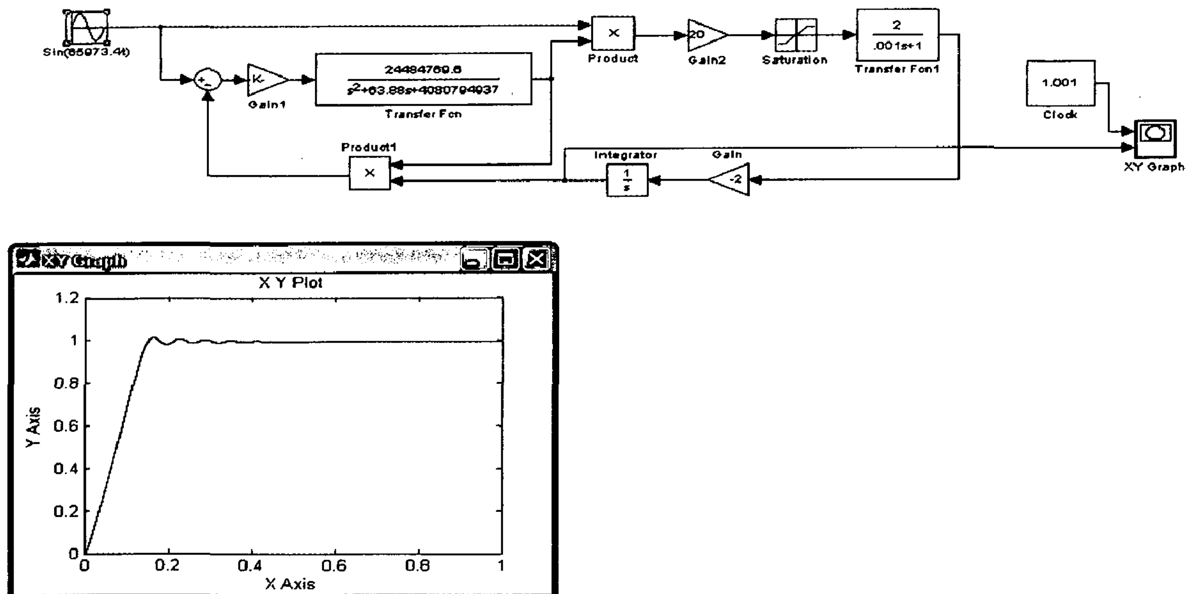

Figure 6.3.3 Adaptive tuning with saturation phase detector and a low pass filter. Graph depicts $\hat{K}$ versus time.

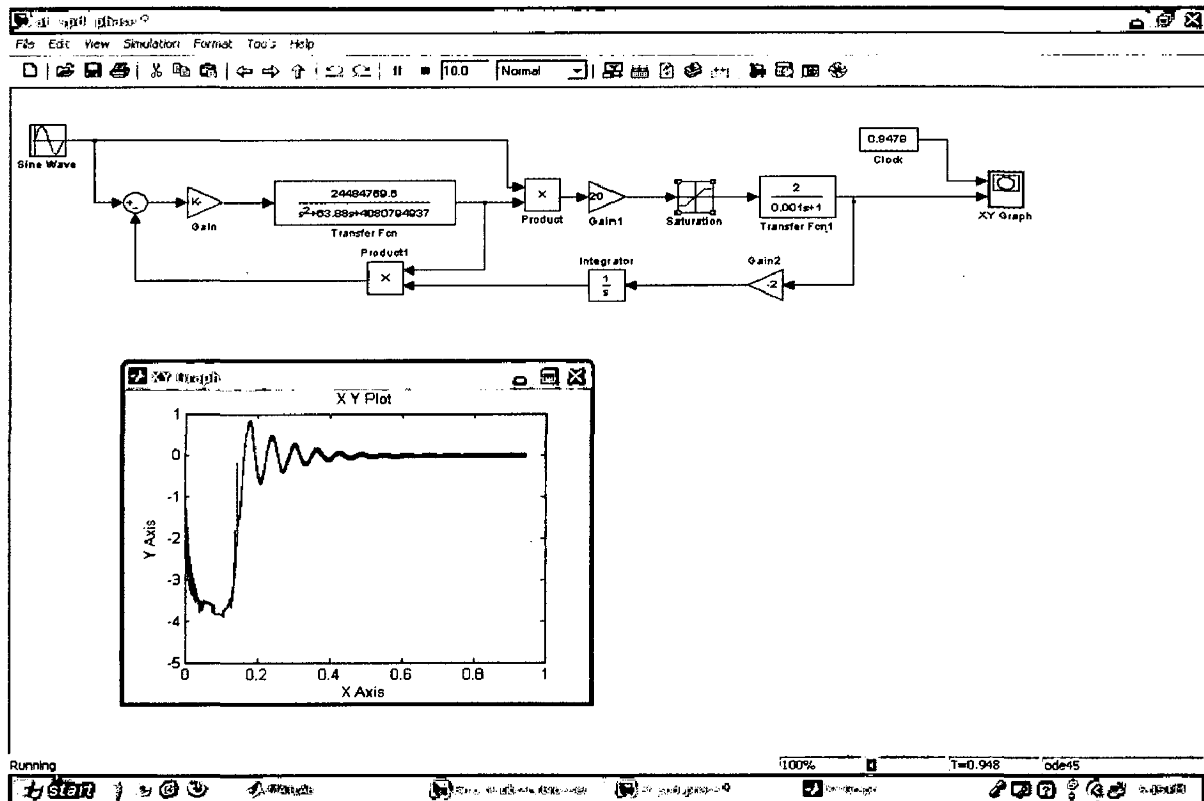

Figure 6.3.4 Adaptive tuning with saturation phase detector and a low pass filter. Graph depicts error input vs time.

As an alternative to a phase locked loop, which produces a periodic signal at the *a priori* unknown resonant frequency of the gyroscope resonator, an adaptive control system is used to alter the system dynamics to place the resonator frequency at a specified frequency. Also, the specified frequency can be easily incorporated into the signal processing design. The use of feedback control in this manner reduces the effect of other fabrication errors. This adaptive control scheme thus helps in tuning the resonant frequency of the drive axis of a vibrational gyroscope.

Conclusion and Future Scope

Gyroscopes are expected to become the next major application for the MEMS industry in the coming years. A multitude of applications already have been developed for consumer and automotive markets. The well known automotive applications are used only in high-end cars, where cost is not a major factor.

The applications for gyroscopes are indeed very broad. Some examples are *automotive*: vehicle stability control, navigation assist, roll over detection, load leveling/suspension control, event recording, collision avoidance; *consumers*: computer input devices, handheld computing devices, gaming controllers, virtual reality gear, sports equipment, camcorders, robots; *industrial*: navigation of autonomous (robotic) guided vehicles, motion control of hydraulic equipment or robots, platform stabilization of heavy machinery, human transporters, yaw rate control of wind-power plants; *aerospace/military*: platform stabilization of avionics, stabilization of pointing systems for antennas, unmanned air vehicles, or land vehicles, inertial measurement units for inertial navigation, and many more.

This dissertation primarily aims for the reader to understand the basic dynamics of an ideal micromachined vibratory gyroscope, error modeling and simulation that may creep in during operation and discusses control strategies for effective utilization of micromachined gyroscope. Theory for an alternative for phase locked loop i.e. adaptive mode tuning is discussed and simulated. With simulations, the dangerous perturbations in a gyroscope that affects the measurement are brought out. The adaptive mode tuning simulation brings out the effectiveness of a saturating phase detector with low pass filter in enabling better phase synchronization.

Primarily due to cost and the size most of these applications have not reached significant volume. New opportunities for design and development of the next generation of low cost and high performance gyroscopes based on the latest MEMS technologies are exploited for commercialization. Production, cost, performance and reliability are the key factors in commercializing micromachined gyroscopes. Precision micromachining, robust vacuum packaging and high performance interface circuit and electronic tuning techniques are required to reduce the production cost to a level that is acceptable for the large volume automotive market.

In general, all silicon, mixed-mode (bulk/surface) fabrication technologies, combined with high aspect ratio deep dry etching techniques, can provide features that are required for future high performance microgyroscopes. Formation of submicrometer capacitive gaps through sacrificial layer etching, high aspect ratio and thick structures with high quality factor and uniform material properties, along with chip-level vacuum package, will help improve the performance by orders of magnitude. Thick, high aspect ratio structures formed by deep dry etching can yield a large sense capacitance with a larger oscillating mass, which in turn will help improve performance and simplify packaging. By shrinking the capacitive gaps to submicrometer levels, bias and control voltages have already shifted to CMOS acceptable levels. High performance tactical and inertial grade gyroscopes are already making use of dynamic electronic tuning of the structure to compensate for temperature and long term drift effects of the sensor.

Progress is made in the development of integrated multiaxis devices on a single chip. In the next decade, much effort will be spent to advance precision machining further, develop low noise and low drift interface circuitry and provide reliable low cost packaging for development of even higher performance, lower cost and lower power inertial sensors for many emerging and as yet unknown applications.

References

1. Anthony Lawrence, "Modern Inertial Technology (Navigation, Guidance and Control), 2nd edition, 1998, Springer publications.

2. C Painter "Micromachined Vibratory Rate Integrating Gyroscopes: Design, Modeling and Experimental Demonstration", Available online in the site www.mems.eng.uci.edu/Personnel/cpainter/format_qual.pdf

3. Jan Soderkvist, "Micromachined gyroscopes", Sensors and Actuators A. 43 (1994) pp.65-71.

4. Navid Yazdi et. al., "Micromachined Inertial Sensors", Proceedings of the IEEE Vol.86, No.8, Aug 1998, pp.1640-1659.

5. Sitaraman V Iyer, "Modeling and simulation of non-idealities in a z-axis CMOS-MEMS gyroscope", Carnegie Institue of Technology, 2003, Available at www.ece.cmu.edu/~mems/pubs/pdfs/ece/phd_thesis/0138_iyer-2003.pdf

6. V Apostolyuk, "Theory and Design of Micromechanical Vibratory Gyroscopes", Available at www.astrise.com

7. B Friedland and M Hutton, "Theory and error analysis of vibrating-member gyroscope", IEEE Transactins on Automatic Control, AC-23(4) pp. 554-556, 1978

8. A Shkel et. al., "Modeling and simulation of micromachined gyros in the presence of imperfection", International Conference on Modeling and Simulation of Microsystems, Puerto Rico, USA, April 1999.

9. Young-Ho Cho et. al., "Slide film damping in laterally driven microstructures", Sensors and Actuators A, 40:31-39, 1994.

10. Igor V. Novozhilov, "Fractional Analysis: Methods of Motion Decomposition", Prentice-Hall, New York, 1995.

11. Larry Baxter, "Capacitive Sensors: Design and Applications", IEEE Press series on Electronics and Technology, 1997.

12. A Shkel et. al., "Dynamics and control of micromachined gyroscopes", Proceedings of the American Control Conference, San Diego, California, 1999.

13. C C Painter and A M Shkel, "Identification of anisoelasticity for electrostatic trimming of rate integrating gyroscopes", SPIE Annual International Symposium on Smart Structures and Materials, San Diego, CA, March 2002.

14. Q Zheng, L Dong and Z Gao, "A novel control system design for vibrational MEMS gyroscopes", Sensors and Transducers Journal, Vol.78, Issue 4, April 2007, pp.1073-1082.

15. S Park and R Horowitz, "Adaptive control for MEMS gyroscopes", Available at http://repositories.cdlib.org/its/path /reports/ UCB-ITS-PRR-2002-11

16. M Kraft, "Micromachined Inertial sensors State of the Art and a Look into the Future, Available online at www.ecs.soton.ac.uk/~mk1/review_pap.pdf

17. Cenk Acar, "Robust Micromachined Vibratory Gyroscopes" Doctoral Dissertation, University of California, Irvine 2004, Available online at www.mems.eng.uci.edu/Personnel/Cenkwebpage/research/cenk_phdthesis_lowres.pdf

18. Robert P Leland, "Adaptive Mode Tuning for Vibrational Gyroscopes", IEEE Transactions on Control Systems Technology Vol 11, No.2, March 2003